

**NASA TECHNICAL
MEMORANDUM**

NASA TM X-3133



NASA TM X-3133

**DISTORTION IN A FULL-SCALE BICONE INLET
WITH INTERNAL FOCUSED COMPRESSION
AND 45 PERCENT INTERNAL CONTRACTION**

*by Joseph F. Wasserbauer, Harvey E. Neumann,
and Robert J. Shaw*

*Lewis Research Center
Cleveland, Ohio 44135*



1. Report No. NASA TM X-3133		2. Government Accession No.		3. Recipient's Catalog No.	
4. Title and Subtitle DISTORTION IN A FULL-SCALE BICONE INLET WITH INTERNAL FOCUSED COMPRESSION AND 45 PERCENT INTERNAL CONTRACTION				5. Report Date December 1974	
				6. Performing Organization Code	
7. Author(s) Joseph F. Wasserbauer, Harvey E. Neumann, and Robert J. Shaw				8. Performing Organization Report No. E-7992	
9. Performing Organization Name and Address Lewis Research Center National Aeronautics and Space Administration Cleveland, Ohio 44135				10. Work Unit No. 501-24	
				11. Contract or Grant No.	
12. Sponsoring Agency Name and Address National Aeronautics and Space Administration Washington, D. C. 20546				13. Type of Report and Period Covered Technical Memorandum	
				14. Sponsoring Agency Code	
15. Supplementary Notes					
16. Abstract <p>An experimental investigation was made to determine the distortion characteristics at the subsonic diffuser exit of a full-scale, Mach 2.5, axisymmetric, mixed compression inlet. Performance and steady-state distortion characteristics were obtained at zero and maximum angle-of-attack and during an inlet unstart-restart sequence. For the configuration with no cowl bleed, steady-state distortion $(P_{\max} - P_{\min})/\bar{P}$ ranged from 0.10 for critical inlet operation at 0° angle-of-attack to 0.306 for supercritical inlet operation at 6.84° angle-of-attack. Vortex generators provided a 50 percent reduction in steady-state distortion for critical operation. Bleed has a smaller effect on steady-state distortion.</p>					
17. Key Words (Suggested by Author(s)) Supersonic cruise inlets Inlets Propulsion systems Inlet flow distortion				18. Distribution Statement Unclassified - unlimited STAR category 28	
19. Security Classif. (of this report) Unclassified		20. Security Classif. (of this page) Unclassified		21. No. of Pages 53	
				22. Price* \$3.75	

DISTORTION IN A FULL-SCALE BICONE INLET WITH INTERNAL FOCUSED COMPRESSION AND 45 PERCENT INTERNAL CONTRACTION

by Joseph F. Wasserbauer, Harvey E. Neumann, and Robert J. Shaw

Lewis Research Center

SUMMARY

An experimental investigation was made to determine the distortion characteristics at the subsonic exit of an axisymmetric mixed compression supersonic inlet. The inlet was designed for Mach 2.5 operation. The external compression was provided by a bi-cone having angles of 12.5° and 18.5° .

Data were obtained over a range of Mach numbers from 2.0 to 2.6. The Reynolds number at the design Mach number was 8.2 million per meter. Performance and distortion characteristics were obtained (1) at zero angle-of-attack, (2) at maximum angle-of-attack (before an inlet unstart occurred) for peak, critical, and supercritical inlet operation, and (3) during an inlet unstart-restart sequence.

With no cowl bleed or vortex generators, the distortion was predominantly a hub radial pattern at the peak terminal shock operating condition. The total pressure recovery was 0.889. At a supercritical terminal shock operating condition, the distortion changed to a predominant tip radial pattern. Adding vortex generators to both the cowl and centerbody resulted in a combined hub-tip radial distortion pattern at the peak operating condition. The total pressure recovery increased to 0.906.

With vortex generators, no cowl bleed, and optimum centerbody bleed flow rates, the maximum angle-of-attack before inlet unstart was 2.55° for supercritical operation and 1.78° for critical inlet operation. The steady-state distortion $(P_{\max} - P_{\min})/\bar{P}$ and maximum angular extent of the distortion for these conditions were 12.5 and 16.0 percent and 175° and 145° , respectively.

When the centerbody bleed flow was increased, an angle-of-attack of 6.84° was obtained before the inlet unstated at supercritical operation. This was, however, a high distortion condition with a steady-state distortion value of 30.6 percent. For critical operation with the centerbody bleed flow rate greater than optimum, an angle-of-attack of 4.17° was obtained before the inlet unstated.

INTRODUCTION

It is well recognized that total pressure distortion at the compressor face is one of the most serious inlet-engine compatibility problems. In order to investigate this area of distortion and associated control problems, an experimental program was conducted in the Lewis 10- by 10-Foot Supersonic Wind Tunnel. An axisymmetric mixed compression inlet with 45 percent of its supersonic area contraction occurring internally was designed for operation with a Pratt and Whitney TF30-P-3 turbofan engine. This report presents the results of the steady-state and root mean square (rms) distortion measurements obtained during a test using a cold-pipe - choked-plug assembly during the development of the inlet. This test was conducted prior to its use with the TF30-P-3 engine.

The tolerance of a turbofan engine to inlet generated total pressure distortion depends on the spatial distribution of the distortion. Circumferential distortions are usually more difficult for an engine to accept than radial distortions. Both the amplitude and the extent of a circumferential distortion are of importance. Recent tests (ref. 1) have indicated that the TF30-P-3 engine is sensitive to angular extents of 180° . This type of distortion is generally obtained in axisymmetric inlets at angle-of-attack. On the other hand, tip radial distortions affect only the outer portion of the fan, which is usually lightly loaded. A turbofan engine is therefore expected to be more sensitive to hub radial distortions because of the direct effect on the core flow. An important part of an inlet development program is therefore the definition of the magnitude and type of the distortion developed at the subsonic diffuser exit.

The test, using the cold-pipe - choked-plug assembly, was conducted over a range of Mach numbers from 2.0 to 2.5. At a Mach number of 2.5, the Reynolds number was 8.2 million per meter. Measurements were made of the distortion at the diffuser exit, the radial distributions of total pressure within the diffuser, the inlet and bleed flow rates, and the total pressure recovery. The maximum angle-of-attack before an inlet unstart was also determined.

U.S. customary units were used in the design of the test model and in recording and computing the experimental data. The units were converted to the International System of units (SI) for use in this report.

APPARATUS AND PROCEDURE

Model

The model installed in the 10- by 10-Foot Supersonic Wind Tunnel is shown in figure 1. The inlet used in this investigation was designed for operation at Mach 2.5. The flow capacity of the inlet was sized for operation with a TF30-P-3 turbofan engine at

Mach 2.5. For this study, however, the inlet was coupled to a cold-pipe - choked-plug assembly. Figure 2 shows the inlet-nacelle combination mounted from the vertical strut in the wind tunnel test section. Figure 3 is an isometric view of the inlet.

The essential features of the inlet were a bicone centerbody of 12.5° and 18.5° half-angle cones and an initial internal cowl angle of 2° . The details of the inlet design are given in references 2 and 3. The design philosophy for this axisymmetric, mixed compression inlet was to utilize a bicone spike to provide the maximum external compression compatible with high total pressure recovery and low cowl drag. As a result, 45 percent of the supersonic area contraction was internal for the Mach 2.5 design condition. The inlet cowl was designed to nearly focus the isentropic compression fan from the cowl and the cowl lip oblique shock on the centerbody bleed slot.

To vary contraction ratio, the design philosophy provided for a collapsing centerbody. The second cone would be collapsed in its lowest position to blend into the first cone contour so as to form a single conic centerbody. For economic reasons, the mechanical design of the test inlet was simplified and the contraction ratio was varied at each test Mach number by centerbody translation rather than by collapsing the centerbody. A second centerbody was designed whose second cone angle is 14.5° as the collapsed version for Mach 2.0 operation (fig. 4).

The supersonic portion of the inlet was designed using an inviscid axisymmetric method of characteristics flow solution. A cross section of the inlet is shown in figure 4. The supersonic diffuser compressed the flow from a Mach number of 2.5 to a throat Mach number of 1.3. A quasi-one-dimensional flow analysis was used to design the subsonic diffuser. The one-dimensional flow area used was based on an assumption of a linear variation in flow angle between the two surfaces. An attempt was made to design the subsonic diffuser for a linear variation of static pressure with axial distance. The terminal shock position was controlled by the flow through a high response bypass door system shown in figure 5. Eight overboard bypass entrances, positioned circumferentially near the diffuser exit, were used. The centerbody was supported by four hollow struts which extended over about one half of the subsonic diffuser length.

The boundary layer development in the inlet was controlled by performance bleed and vortex generators. The provision for cowl boundary layer bleed was provided by holes perpendicular to the surface located both forward and aft of the geometric throat as shown in figures 4 and 6. As discussed in reference 2, this bleed was found to be unnecessary for good performance. Nevertheless, the results of the cowl bleed study are presented herein in so far as they affect the distortion study. The cowl bleed configurations tested are shown in figure 7. Centerbody performance bleed was provided by a slot at the cone shoulder. This bleed flow, ducted internally through the centerbody, passed through the four hollow struts, and was throttled by choked butterfly valves at the exit of the struts. Results from each of the centerbody bleed configurations shown in figure 8 are presented. Vortex generators were provided on both the centerbody and the cowl to inhibit separation

by energizing the low energy flow near the walls. The vortex generators were located at an $x/R_c = 3.37$ and are pictured in figure 6. (Symbols are defined in appendix A.) The definition of the performance bleed and vortex generator configuration nomenclature is given in appendix B.

All cowl bleed configurations were tested with centerbody bleed configuration A (fig. 8(a)) and with vortex generators on the cowl and the centerbody. Centerbody configuration A was also tested with the porous cowl bleed sealed. The flush slot of configuration A was designed for a maximum bleed mass flow ratio of about 0.07 of the inlet capture flow. The ram-scoop slot configurations with blunt and sharp lips were designed to operate on design with a bleed mass flow ratio of 0.03 and are shown in figures 8(b) and (c). For all tests with the ram-scoop slot configurations, the cowl bleed was sealed and no vortex generators were used in the subsonic diffuser. Details of the vortex generators used on the cowl and centerbody are shown in figure 9.

Instrumentation

Steady-state and dynamic instrumentation at the diffuser exit is shown in figure 10. Each rake contained six equal area-weighted total pressure tubes. The overall diffuser exit total pressure recovery was determined from the twelve six-tube rakes. The angular location of the twelve rakes has been adjusted for the presence of the four struts. This resulted in a 2.5° correction on eight of the twelve rakes. Wall static pressure measurements were made using the 20 wall static taps shown in the figure.

In order to measure the fluctuating component of total pressure, subminiature absolute pressure transducers were mounted in the rakes at the three locations shown in figure 10. The transducers were mounted in the rakes such that a simultaneous steady-state and fluctuating pressure measurement could be made. The resultant configuration provided a flat response to at least 1000 hertz. The output signal was passed through a second-order low pass filter with a 1000-hertz corner frequency and measured with a true rms meter.

At each steady-state operating condition, fluctuating pressures were recorded at each of the three locations shown in figure 10. The average value of the associated rms measurements of the fluctuating component of total pressure was ratioed to the average steady-state recovery pressure. This ratio is defined herein as the dynamic distortion level for that particular operating condition.

Test Procedure

A number of inlet operating conditions were investigated for each inlet configuration. Data were obtained for peak, subcritical, critical, and supercritical operation. Peak operation is defined as the minimum stable condition with the terminal shock at its most forward position in the inlet. Critical operation is defined as the terminal shock position at the inlet's geometric throat. Operation with the terminal shock between the throat and the most forward position is defined to be subcritical operation. Supercritical operation is hence defined as operation with the terminal shock downstream of the throat.

At the inlet design Mach number and contraction ratio and at zero angle-of-attack, a centerbody bleed flow rate was determined to obtain the maximum total pressure recovery for critical inlet operation. This centerbody bleed flow rate is referred to herein as the optimum centerbody bleed flow rate. Data were also taken for various overboard bypass flows (when the bypass system was operating) at the match compressor face corrected airflow required for the TF30-P-3. This match compressor face airflow occurs at critical inlet operation. Data were also taken at various compressor face corrected airflows by varying the choked-plug area while keeping the bypass area at the original match point setting or with the overboard bypass system sealed. Results were also obtained for values of centerbody bleed flow greater than optimum while the inlet was operating in a subcritical condition.

The maximum attainable angle-of-attack was determined with the inlet operating in a steady-state mode for both optimum and increased centerbody bleed. This maximum angle-of-attack data was obtained for a minimum stable condition when the inlet was operated at subcritical, critical, and supercritical terminal shock positions.

Although the design philosophy involved a collapsing centerbody to vary the internal contraction ratio, data were taken to define the distortions associated with the subsonic diffuser as the contraction ratio was varied by centerbody translation during the unstart-restart sequence. These data were obtained at various values of cowl-lip-position parameter from the stable unstarted condition to an operating point just before restart. Data were also taken with the inlet started at equivalent points as the inlet returned to the design operating point. All data obtained during the inlet unstart-restart cycle sequence were for steady-state stable operation.

RESULTS AND DISCUSSION

The results presented herein are for three different operating conditions. The first set of results are for operation at zero angle-of-attack. The second section is for operation at maximum angle-of-attack. The final set of results are for an unstart-restart sequence at zero angle-of-attack.

Vortex generator effects on performance and distortion. - The performance of the inlet at zero angle-of-attack without and with vortex generators on both the cowl and centerbody is shown in figure 11. The data shown are for an inlet configuration with no cowl bleed or overboard bypass flow. The centerbody is configured with the flush slot centerbody bleed configuration of figure 8(a). These configurations are called configurations A and Accb (see appendix B).

The improvement of performance resulting from the use of vortex generators in the subsonic diffuser is shown in figure 11. As is well known, the vortex generators re-energize the low energy flow near the walls. This improves the efficiency of the diffusion process and for this inlet results in an increase in total pressure at the diffuser exit. As is shown in the figure, the recovery for peak operation increases from 0.889 to 0.906.

The apparent increase in dynamic distortion resulting from the use of vortex generators presented in the figure is due to the limited instrumentation. The level of dynamic distortion is related to the gradient in recovery as discussed in reference 4. Since the three dynamic measurements are all made in regions of high pressure recovery and low pressure gradient (center annulus), the low values of dynamic distortions are not representative of the spatial average at the diffuser exit at peak and critical operation for the configuration without vortex generators. When the vortex generators are added to the subsonic diffuser, not only is the low energy air near the walls re-energized but the regions of high recovery are de-energized. As a result of this mixing of the flow, the level of the fluctuations in recovery increases in regions of high recovery.

The vortex action also reduces the spatial gradients in recovery at the diffuser exit. This is evidenced by the 50 percent reduction in steady-state distortion from a value of about 0.2 to about 0.1 for both critical and peak operation.

The effect of the vortex generators can be seen more clearly by replotting the data of figure 11 in terms of the axial position of the terminal shock system, as shown in figure 12. Data are shown for operation at the design inlet Mach number of 2.5, with and without vortex generators in the subsonic diffuser. The performance of the inlet with the centerbody which was designed for operation at Mach 2.0 (with vortex generators) is also presented. As mentioned previously, this centerbody simulates the collapsed configuration.

Figure 12 also shows that the mixing induced by the vortex action of the generators is sufficient to cause a redistribution of the high energy flow such that an increase in recovery is obtained. The re-energizing of the low energy air near the walls also results in a reduction in steady-state distortion of 0.1. Although the vortex generators reduce the level of distortion, they do not affect the qualitative shape of the curve of the variation of distortion with terminal shock position. The sudden increase in distortion at an

x/R_c of about 3.5 is due to a change in distortion contour and occurs when operating both with and without vortex generators.

The level of dynamic activity at the diffuser exit is strongly dependent on the location of the terminal shock relative to the vortex generator station, as is shown in figure 12. The dynamic activity, as indicated by the dynamic distortion level, is low for shock positions upstream of the vortex generator station. When the terminal shock is downstream of the vortex generator station, large increases in dynamic distortion are encountered. As previously discussed, the indicated level of dynamic distortion with vortex generators is higher than without generators because of the limited dynamic instrumentation. The indicated level of dynamic distortion observed with the collapsed Mach 2.0 configuration is similar to that obtained at Mach 2.5.

The steady-state distortion contours at the diffuser exit are shown in figure 13 for four different terminal shock positions for configuration Accb. These contour plots represent a qualitative measure of the spatial distribution of total pressure as measured by the twelve rakes at the diffuser exit. The measured pressures are spatially faired by a computer program such that the presence of the four support struts are ignored. The position of these support struts are indicated in the contour plots. Since the diffuser flow is channeled by the inlet struts, secondary flows are present in the strut region (ref. 5). These secondary flows are a result of radial static pressure gradients. The static pressure on the cowl is generally slightly larger than on the centerbody in the strut region. This pressure gradient causes a radial flow along each surface of the struts inward toward the centerbody. Two secondary flow cells result with an accumulation of low total pressure flow on the centerbody between two adjacent struts.

When the terminal shock is upstream of the vortex generators, the distortion patterns of figure 13 are similar. The distortions are radial with little evidence of strut induced secondary flows. The static pressure in the strut region on the cowl are an average of 1.5 percent greater than those on the centerbody. With the terminal shock downstream of the vortex generators, the radial static pressure gradients increase and have a larger effect on the low energy air. The static pressure on the cowl is about 6 percent greater than on the centerbody. Circumferential distortion and the strut induced secondary flows then begin to appear. At extreme supercritical operating conditions the steady-state distortion patterns become both radial and circumferential. Large strut effects are evident.

For operation at peak recovery without vortex generators (configuration A), the flow separates in the subsonic diffuser on the centerbody (fig. 14(a)). This results in a region of relatively low total pressure recovery at the hub. For this operating condition the distortion is radial with the highest recovery occurring near the cowl. When the terminal shock is at the throat and downstream of the throat, the separation occurs on the cowl (figs. 14(b) and (c)). Secondary flows due to the four struts also result. This results in low recovery on the cowl and nonuniformity in the circumferential direction. Despite the

existence of secondary flows, the distortion at the diffuser remains predominantly radial when operating without vortex generators.

Bleed effects on distortion. - The effect of centerbody bleed and spike position on distortion is presented in figure 15. The results presented are for a free stream Mach number of 2.5. For each centerbody bleed configuration tested, a reduction in cowl-lip-position parameter (i. e., centerbody moved forward) resulted in a slight increase in both steady-state and dynamic distortion. Small increases in peak recovery were also observed to occur, but at the expense of more mass flow spilled over the cowl. The steady-state distortion levels are similar for all three configurations.

The effects of the various cowl bleed configurations on distortion are shown in figure 16. The centerbody bleed configuration A was used with each cowl bleed configuration, and vortex generators were installed on both the cowl and centerbody. Performance and distortion results are presented in the figure, for a free stream Mach number of 2.5. Bypass flow variation was at the match TF30 engine corrected airflow. The trends in recovery and distortion were similar with and without cowl bleed. With cowl bleed and optimum centerbody bleed, total pressure recoveries at critical inlet operation were higher than without cowl bleed. As a result, higher engine mass flow ratio (less overboard bypass flow) was obtained at the match condition (critical inlet operation). A more complete discussion of the differences in the bleed configurations is given in reference 4. The steady-state distortion was nearly identical for the four bleed configurations and for the configuration without cowl bleed except at extreme supercritical operating conditions. The dynamic distortion was about 2 percent for all conditions except for extreme supercritical operation.

The steady-state distortion patterns for bleed configuration IAcCb are given in figure 17. Distortion patterns for the other configurations are similar. The distortion patterns for peak operation, with either optimum centerbody bleed flows or increased bleed flow, shows that there is virtually no distortion. Only a very small radial distortion exists. When the terminal shock is moved downstream of the vortex generators, the radial distortion increases. For supercritical operation at a recovery of 0.851, the patterns begin to show strut induced secondary flows. As was discussed earlier, these secondary flows begin to become evident when the terminal shock moves downstream of the vortex generators. The distortion pattern for supercritical operation at a given recovery level is the same with or without overboard bypass flow. At extreme supercritical operation, the distortion pattern becomes mixed radial and circumferential. Large secondary flows are evident.

Effect of overboard bypass flow. - The effect of overboard bypass flow on performance is obtained by a comparison of the results presented in figures 11 and 16(a). The results of figure 16(a) are presented for operation at Mach 2.5 with configuration AcCb, and overboard bypass flow. The results presented in figure 11 are for configuration AcCb without overboard bypass flow. Peak recovery at optimum centerbody bleed

decreased from 0.905 (see fig. 11) to 0.895 with bypass flow. The 8.0 percent over-board bypass flow is necessary to match the TF30 engine requirements. The steady-state distortion increased by about 1 percent with bypass flow. The increased distortion may be caused by the operation of the bypass doors. The bypass doors are located in the diffuser region where the area ratio changes rapidly. Because of this rapid area variation, strong adverse pressure gradients are present and tend to separate the flow. Bypassing diffuser flow through the bypass system only adds to the severity of the pressure gradient and tends to further promote separation. Further details are presented in reference 3. The dynamic distortion based on a three probe measurement remained unchanged. Results obtained with other cowl bleed configurations are similar to those presented in figure 16(a).

Free stream Mach number effects. - The inlet was tested over a range of free stream inlet Mach numbers. The simulated Mach 2.0 collapsed configuration was tested at Mach 2.0 and 2.1, whereas the Mach 2.5 design configuration was tested at Mach numbers of 2.3, 2.4, 2.5, and 2.6. The performance at these Mach numbers is given in figure 18. Bypass flow variation at the various Mach numbers was performed at the match TF30 corrected airflows. With the Mach 2.5 centerbody, as the off design Mach number increased from 2.4 to 2.6, the total pressure recovery decreased and the mass flow ratio increased for operation at critical terminal shock position. The recovery at peak operation with increased centerbody bleed was lower at off design Mach numbers of 2.4 and 2.6 than at design conditions. The recovery at Mach 2.3 operation is generally slightly less than at Mach 2.4 operation because the inlet is operating farther from design operation.

The steady-state distortion was not affected by changes in inlet Mach number from 2.3 to 2.5. The decrease in steady-state distortion above a recovery of about 0.825 for each Mach number condition from 2.3 to 2.5 was a result of a changing distortion pattern. The distortion associated with recoveries greater than 0.825 is hub radial. For more supercritical operation, the distortion changes to a pattern with a large circumferential component. The steady-state distortion at Mach 2.6 is slightly higher than at lower Mach numbers.

The performance of the Mach 2.0 collapsed centerbody configuration of the centerbody is given in figures 18(e) and (f). The peak recovery was 0.96 at increased centerbody bleed. This value of recovery was obtained at both Mach 2.0 and 2.1. The recovery at the match corrected airflow for the TF30-P-3 was 0.935 at both Mach numbers. The steady-state distortion is governed by secondary flow interacting with the low energy flow on the centerbody for Mach numbers of 2.0 and 2.1. The resultant steady-state distortion pattern is similar to the pattern shown in figure 17 for supercritical operation at a recovery of 0.871. The flow near the cowl had high recovery. This high recovery near the cowl is present whenever the average recovery is 0.90 or higher. A large region near the cowl had local values of recovery in excess of 0.96.

At Mach 2.0 operation and a total pressure recovery of about 0.90, the steady-state distortion suddenly decreases, as shown in figure 18(f). This reduction is reflected in a change in the radial distortion. The radial distortion, as measured by the radial distortion index K_{ra} is reduced from a value of 0.37 at a recovery of 0.907 to a value of 0.20 at a recovery of 0.874. The circumferential distortion remains about the same for these conditions. The circumferential distortion as measured by K_{θ} remains at a level of about 0.04. For both conditions, these results are for variations in performance as the overboard bypass flow is varied. Similar results are obtained for an exit plug variation. (K_{θ} and K_{ra} are defined in appendix C).

As the terminal shock moves downstream, the mass flow ratio at the diffuser exit increases as is shown in figures 18(e) and (f). This increase in mass flow ratio is a result of changes in the overboard bypass mass flow. For operation at Mach 2.0, a bypass flow ratio of 0.11 is necessary to match TF30-P-3 engine requirements. As the terminal shock moves to a more supercritical position, the recovery decreases and results in a reduction in pressure ratio across the overboard bypass. This results in less bypass flow as indicated in figure 18(f). As a consequence of continuity requirements, however, the sum of the diffuser exit mass flow ratio and the bypass mass flow ratio remain constant. This sum is also shown in figure 18(f). It should be noted that this effect on the overboard bypass flow is much reduced for operation at Mach 2.5 (figs. 16(a) to (d)) due to the small amount of bypass flow.

Operation at Angle-of-Attack

For normal inlet operation the terminal shock is positioned at or near the inlet throat. Inlet operation with the terminal shock downstream of the throat (supercritical operation), is used when an anticipated maneuver is about to be made. The inlet angle-of-attack data for these two operating conditions are presented in table I and figure 19. Data were obtained at both the optimum and increased centerbody bleed flow rates. The inlet's steady-state performance, various steady-state distortion parameters, and the dynamic distortion parameter are presented in the table for the various inlet configurations. In the table, K_{θ} is the steady-state circumferential distortion parameter and K_{ra} is the steady-state radial distortion parameter. The parameter entitled angular extent is the maximum circumferential region of total pressure having values less than the average in either a tip, mean, or hub ring. The two outer rings of total pressure measurements (fig. 10) at the diffuser exit were averaged to represent the tip ring. Likewise, the two inner rings of total pressure measurements were used to represent the hub ring. The mean ring was based on the two middle rings of total pressure measurements. For each of the three resultant rings, the extent of pressure below the ring average was determined. The largest of the three extents is listed in table I.

The following procedure was used to obtain the angle-of-attack data. For maximum angle-of-attack at critical inlet operation and with the optimum centerbody bleed flow: (1) the inlet was set at the critical operating point for 0° angle-of-attack, and (2) the model angle-of-attack was increased until an unstart occurred. The inlet was restarted and data were then recorded for an angle slightly less than the unstart angle-of-attack. This is a minimum stable condition for critical inlet operation. Angle-of-attack for peak inlet operation follows the same procedure as for critical operation.

For maximum angle-of-attack at supercritical inlet operation: (1) the inlet mass flow plug was fully retracted, (2) the model angle-of-attack was increased until an unstart occurred, (3) the inlet was restarted and the model angle-of-attack was set slightly less than the unstart angle, (4) the mass flow plug was then closed until the inlet unstarted, (5) after the inlet was restarted, the plug was relocated near the position causing unstart. This data point is defined as the minimum stable condition for supercritical inlet operation. For angle-of-attack operation with increased centerbody bleed flow, the same procedure was used for peak, critical, and supercritical inlet operation.

Critical operation. - The angle-of-attack performance for the critical inlet operating points is given in table I(a). Without an operating bypass system, configuration A (no cowl bleed) compared with configuration Accb at optimum and near capacity centerbody bleed flow rates shows that all distortion parameter values decreased when the vortex generators were added. With an operating bypass system, the highest critical angle-of-attack was 4.17° for configuration Accb when the full capacity of the centerbody bleed system was used. However, when cowl bleed was added, configuration II Accb operated at 7.19° with maximum centerbody bleed. This result can be seen by comparing figures 19(c) and (d). Small differences in the values of the distortion parameters were indicated when comparing the cowl bleed configuration II Accb with the no bleed configuration Accb at their respective angle-of-attack operating limits. The exception was the parameter K_θ which increased in value for the higher angles-of-attack of configuration II Accb. As shown in the table, larger angle-of-attack operation is possible when cowl bleed is used but not without large circumferential distortions K_θ . When operating at angle-of-attack, the circumferential distortion was always much larger than the radial distortion. Also, for each configuration, the circumferential distortion always increased as the angle-of-attack was increased.

In addition to the stronger circumferential patterns when at angle-of-attack, secondary flows due to the struts are in evidence. These secondary flows can be seen in figure 19(a) on the centerbody in sectors at about $\pm 90^\circ$ with respect to the vertical. The low pressure located on the centerbody in the vertical position arises from the combined effects of angle-of-attack and secondary flows.

Supercritical operation. - A summary of the performance and distortion at angle-of-attack for supercritical operation is given in table I(b). Large steady-state distortions were encountered for operation at Mach 2.5 with supercritical terminal shock positions.

The circumferential component of distortion is generally quite high with K_θ values reaching 0.749 for operation at the design Mach number of 2.5. The high loss region on the windward (bottom) side extends to about one half the annulus area at the diffuser exit as shown in figures 19(e) to (g). Secondary flows due to strut effects are still present even at the large angles-of-attack as shown in figures 19(e) and (f). The radial component of distortion is low even when the Mach 2.0 centerbody was used. For Mach 2.0 centerbody operation, radial distortion K_{ra} varied from 0.291 to 0.472 for the angle-of-attack conditions measured.

Angular extent. - The angular extent of the below average total pressure is given in figure 20 for the hub, mean, and tip rings as defined previously. The data presented are for critical operation in figure 20(a) and for supercritical operation in figure 20(b). Both sets of data are for operation at Mach 2.5 and at the design cowl-lip-position parameter of 26.4° . Large circumferential extents of pressure below average are noted at critical operations. Near the tip the extent is about 175° . At supercritical operation, the maximum extent diminishes only slightly. For both operating conditions the radial variation of the extent does not change appreciably. The maximum extent for each angle-of-attack data point is listed in table I.

Effect of vortex generators. - The effect of vortex generators on the performance at angle-of-attack is shown in figures 21(a) and (b). The total pressure recovery, steady-state distortion, circumferential distortion, and dynamic distortion variations with angle-of-attack are presented for configurations A and Accb. The data shown is for minimum stable angle-of-attack operation. Results for both optimum centerbody bleed flow and increased centerbody bleed flow rates are shown. The area between the two curves represents the increase in angle-of-attack obtained when the centerbody performance bleed is varied from its optimum value to the maximum capacity. Without generators, the circumferential distortion parameter K_θ was nonlinear and increased very rapidly at small angles-of-attack (fig. 21(a)). With vortex generators, higher recoveries and lower distortions were obtained. Furthermore, the variation of circumferential distortion parameter K_θ varied almost linearly with angle-of-attack. Dynamic distortion was approximately linear with angle-of-attack when the inlet operated with and without vortex generators. The dynamic distortion was reduced at large angle-of-attack operation when vortex generators were used.

Effect of cowl bleed. - The effect of cowl bleed on angle-of-attack performance is shown by comparing the results presented in figures 21(b) and (c). Results using bleed configuration IAccb are presented and compared with bleed configuration Accb. In all cases shown, larger angles-of-attack were attainable with cowl bleed than without. The maximum angle obtainable without cowl bleed was 6.84° . With cowl bleed, this angle increased to 7.83° . At this condition the inlet did not unstart but rather the maximum model support strut angle-of-attack was reached. At small angles-of-attack, the recoveries at optimum bleed operation were essentially the same with or without cowl bleed.

At increased centerbody bleed flows, the performance with cowl bleed surpassed the performance without bleed. At increased angles-of-attack, the pressure recovery did not decrease as rapidly with changes in angle-of-attack when the cowl was bled. The steady-state and dynamic distortion were also less with cowl bleed than without.

When bleed was used on both the cowl and the centerbody, the amount of centerbody bleed had a significant effect on steady-state distortion $[(P_{\max} - P_{\min})/\bar{P}]_2$. The effect was most pronounced at zero angle-of-attack. The steady-state distortion was reduced from 0.105 to 0.030 as the centerbody bleed flow was increased from optimum to the increased flow rate. The circumferential distortion index K_θ showed a modest reduction when cowl bleed was used.

Effect of Mach number. - The effects of free stream Mach number changes on distortion at angle-of-attack is shown in figures 21(c) and (d). The performance shown in figure 21(c) for the Mach 2.5 configuration was also about the same for operation at Mach 2.4. At Mach 2.5, the distortion values $[(P_{\max} - P_{\min})/\bar{P}]_2$ were lower and the K_θ values higher when compared to Mach 2.0 operation. However, the maximum attainable angle-of-attack was substantially reduced for operation with the Mach 2.0 configuration. The recovery for operation with the Mach 2.0 centerbody configuration was higher than for the Mach 2.5 operation over the entire operating range of angle-of-attack.

Unstart-Restart Sequences

The distortion and performance of the inlet during an unstart-restart sequence is shown in figures 22 and 23. The data presented in the figures were obtained as the cowl-lip-position parameter was varied by centerbody translation. It should again be mentioned that this inlet was not intended to utilize centerbody translation but rather was designed to utilize a collapsing centerbody to vary contraction ratio. However, for a flight-type inlet some combination of collapsing and translating the centerbody may be desirable to restart the inlet.

The sequence was started by setting the inlet for a critical terminal shock position and optimum centerbody bleed flow rate. The exit plug and centerbody bleed were held fixed for the entire sequence. The inlet was unstarted by pulsing the bypass doors closed and then the bypass flow adjusted to determine the point of incipient buzz. This point at the design cowl-lip-position parameter is labeled the "beginning of unstart, minimum stable unstart point without buzz." At this point, the bypass door exit area was slightly larger than for the started inlet condition. For the midexcursion unstarted point θ_l of 25° , the bypass doors were reset to the original exit area without encountering "buzz." This bypass door exit area remained fixed for the remainder of the sequence since "buzz" was not encountered. No attempt was made to determine minimum stable conditions through the sequence except for the initial condition.

The cowl-lip-position parameter was then reduced (centerbody extended) until the inlet was at incipient restart. This point is called the "just before restart" point. The inlet was then restarted and set at the same cowl-lip-position parameter as the previous unstarted point. This point is labeled the "just after restart" point. Returning to the design cowl-lip-position parameter with started operation is the "end of unstart sequence, started operation" operating point.

The steady-state distortion patterns shown in figure 22 remain radial for the entire unstart-restart sequence. At the initial minimum stable operating condition with unstarted operation, the largest total pressure loss occurs near the centerbody. With the inlet remaining unstarted, large losses in recovery are noted on both the centerbody and the cowl as the cowl-lip-position parameter is decreased. This general distortion pattern persists for all cowl-lip-position parameters with the inlet in a started mode of operation. The recovery is much lower, however, for unstarted operation than for a started mode of operation.

Total pressure recovery, overboard bypass mass flow ratio, radial and circumferential distortion indices, and steady-state distortion are presented in figure 23 for operation at design free stream Mach number. The total pressure recovery decreased as the cowl-lip-position parameter decreased with the inlet operating in a started mode of operation. The maximum steady-state distortion occurred with the inlet started and the centerbody positioned at intermediate values of cowl-lip-position parameter.

The circumferential distortion index K_θ was largest during unstarted operation and had a maximum value of about 0.2. With the inlet in a started mode of operation, K_θ was less than 0.06 for all cowl-lip-position parameters. Significant variations in radial distortion were noted during the unstart-restart sequence. The radial distortion was largest during the started mode of operation. The radial distortion index K_{ra} exceeded values of 50 percent during the restart sequence. These large values of radial distortion did not persist over the entire sequence however. The smallest values of radial distortion occurred during unstarted operation at cowl-lip-position parameters just before restart. The minimum values of radial distortion were less than 10 percent.

When the inlet unstarts at design operation, the radial distortion index becomes very large. A value of 0.51 is attained. If an engine is sensitive to this level of radial distortion, the level can be reduced by decreasing the overboard bypass flow as the inlet unstarts. This also results in a decrease in the steady-state distortion but an increase in the circumferential distortion. Another potentially high risk condition arises after the inlet is restarted. At reduced cowl-lip-position parameters, both large values of steady-state and radial distortion are encountered. If the engine is sufficiently sensitive to these levels of distortion, the inlet could reinitiate an engine stall-inlet unstart sequence and hence also initiate a nonrecoverable sequence of events. It should be re-emphasized that this inlet was designed for a collapsing configuration, however, and not the translating configuration tested herein. This same problem exists at off design operating

conditions where the maximum distortion often occurs just after restart. This creates a potential problem area for restarting an engine. Engine-inlet compatibility problems of this nature are of course beyond the scope of this investigation and must be further investigated in engine tests.

SUMMARY OF RESULTS

An experimental investigation was made to determine the distortion characteristics at the subsonic exit of an axisymmetric mixed compression supersonic inlet. The inlet was designed for Mach 2.5 operation. The external compression was provided by a bi-cone having angles of 12.5° and 18.5° . Fifty-five percent of the supersonic area contraction occurred externally.

Data were obtained over a range of Mach numbers from 2.0 to 2.6. The Reynolds number at the design Mach number was 8.2 million per meter. Performance and distortion characteristics were obtained (1) at zero angle-of-attack, (2) at maximum angle-of-attack (before an inlet unstart occurred) for peak, critical, and supercritical inlet operation, and (3) during an inlet unstart-restart sequence. The following results were obtained:

1. With no cowl bleed or vortex generators, the distortion was predominantly a hub radial pattern at the peak terminal shock operating condition. The total pressure recovery was 0.889. At a supercritical terminal shock operating condition, the distortion changed to a predominant tip radial pattern. Adding vortex generators to both the cowl and centerbody resulted in a combined hub-tip radial distortion pattern at the peak operating condition. The total pressure recovery increased to 0.906. When the terminal shock was moved downstream to a supercritical operating condition, the distortion pattern became a combined radial-circumferential pattern. This was a result of a strong secondary flow on each of the four diffuser support struts.

2. When cowl bleed was added, the effects on steady-state distortion were small for peak inlet operation. When the centerbody bleed flow rate was increased, the steady-state distortion decreased, the pattern became only slightly hub radial, and the recovery increased to 0.942. The steady-state distortion levels were less than 15 percent except at extreme supercritical terminal shock positions.

3. With vortex generators, no cowl bleed, and optimum centerbody bleed flow rates, the maximum angle-of-attack before inlet unstart was 2.55° for supercritical operation and 1.78° for critical inlet operation. The steady-state distortion $[(P_{\max} - P_{\min})/\bar{P}]_2$ and maximum angular extent of the distortion for these conditions were 12.5 and 16.0 percent and 175° and 145° , respectively.

When the centerbody bleed flow was increased, an angle-of-attack of 6.84° was obtained before the inlet unstated at supercritical operation. This was, however, a high distortion condition with a steady-state distortion value of 30.6 percent. For critical operation with the centerbody bleed flow rate greater than optimum, an angle-of-attack of 4.17° was obtained before the inlet unstated.

With cowl bleed, the attainable angles-of-attack increased. The steady-state distortion levels tended to also increase. With optimum centerbody bleed flow rates, the maximum angle-of-attack was 4.96° for supercritical operation and 3.49° for critical inlet operation. The steady-state distortion levels for these two conditions were 13.5 and 21.7 percent.

The distortion patterns of the previously summarized angle-of-attack conditions were circumferential. The circumferential distortion index K_{θ} generally increased with angle-of-attack. Radial distortion levels were generally low.

4. The maximum steady-state distortion during an unstart-restart sequence occurred at off design cowl-lip-position parameters slightly larger than the restart value. The distortion pattern was a combined hub-tip radial. This maximum steady-state distortion was 6 percent larger than the distortion present at design cowl-lip-position parameter.

Lewis Research Center,
National Aeronautics and Space Administration,
Cleveland, Ohio, July 10, 1974,
501-24.

APPENDIX A

SYMBOLS

d	distance from centerbody
H	annulus height at local diffuser station
K_{ra}	radial distortion index (see appendix C)
K_{θ}	circumferential distortion index (see appendix C)
M	Mach number
m/m_0	mass flow ratio
P	total pressure
ΔP	fluctuating component of total pressure
R_c	cowl lip radius
r	local radius
x	axial location
α	angle-of-attack
θ_l	cowl-lip-position parameter, $\arctan (R_c/x)$, deg

Subscripts:

by	bypass
cb	centerbody
max	maximum
min	minimum
rms	root mean square
st	strut
0	free stream inlet station
2	diffuser exit station

Superscript:

—	area weighted average
---	-----------------------

APPENDIX B

CONFIGURATION NOMENCLATURE

The cowl bleed configurations are shown in figure 7 and are represented by Roman numerals. The centerbody bleed configurations are shown in figure 8 and are represented by capital letters. The use of vortex generators is indicated by either cb or ccb. If generators are used on the centerbody only, the designation cb is used. If generators are used on both the centerbody and the cowl, the designation ccb is used. For example, the configuration IAcbb indicates that cowl configuration I is used with centerbody bleed configuration A and vortex generators were used on both the cowl and the centerbody. If a configuration designation is omitted, the bleed represented by that designation is not used.

APPENDIX C

DEFINITIONS

Pratt and Whitney Distortion Factor K_θ

The distortion factor K_θ is defined by the following equation

$$K_\theta = \frac{\sum_{i=1}^6 \left[\left(\frac{A_N}{N^2} \right)_{\max} \right]_i \frac{1}{D_i}}{\frac{Q}{P_{av}} \sum_{i=1}^6 \frac{1}{D_i}}$$

where

$$\left(\frac{A_N}{N^2} \right)_i = \left[\frac{1}{N^2} \sqrt{a_N^2 + b_N^2} \right]_i \quad N = 1, 2, 3, \dots$$

$$a_N = \frac{1}{\pi} \int_{-\pi}^{\pi} \frac{P}{P_{av}} \cos N\theta \, d\theta$$

$$b_N = \frac{1}{\pi} \int_{-\pi}^{\pi} \frac{P}{P_{av}} \sin N\theta \, d\theta$$

P local compressor face total pressure

D_i local compressor face diameter

Q compressor face dynamic pressure

P_{av} average compressor face total pressure

Radial Distortion Index K_{ra}

The radial distortion index is defined by the following equation

$$K_{ra} = \frac{\sum_{i=1}^6 \frac{DP}{P_{av}} \left(\frac{1}{D_i} \right)^{2.8}}{\frac{Q}{P_{av}} \sum_{i=1}^6 \left(\frac{1}{D_i} \right)^{2.8}}$$

where

DP $P_{av} - P_{i,av}$; if DP is negative, DP is set to zero

P_{av} average compressor face pressure

$P_{i,av}$ local ring average of P_i

P_i local compressor face total pressure on i^{th} ring

Q compressor face dynamic pressure

D_i local compressor face diameter

REFERENCES

1. Wenzel, Leon M.: Experimental Investigation of the Effects of Pulse Pressure Distortion Imposed on the Inlet of a Turbofan Engine. NASA TM X-1928, 1969.
2. Wasserbauer, Joseph F.; Shaw, Robert J.; and Neumann, Harvey E.: Minimizing Boundary Layer Bleed for a Mixed Compression Inlet. Paper 73-1270, AIAA, Nov. 1973.
3. Wasserbauer, Joseph F.; Shaw, Robert J.; and Neumann, Harvey E.: Design of a Very-Low-Bleed Mach 2.5 Mixed-Compression Inlet with 45 Percent Internal Contraction. NASA TM X-3135, 1974.
4. Calogeras, James E.; Burstadt, Paul L.; and Coltrin, Robert E.: Instantaneous and Dynamic Analysis of Supersonic Inlet-Engine Compatibility. NASA TM X-67821, 1971.
5. Schlichting, Herman: Boundary Layer Theory. 6th ed., McGraw-Hill Book Co., 1968, pp. 575-578.

TABLE I. - PERFORMANCE AND DISTORTION AT ANGLE-OF-ATTACK

(a) Critical terminal shock position

Configuration	Inlet Mach number, M_0	Centerbody bleed, m_{st}/m_0	Cowl bleed, m_{cb}/m_0	Performance			Distortion				
				Total pressure recovery, \bar{P}_2/P_0	Mass flow ratio, m_2/m_0	Angle-of-attack, α , deg	$[(P_{\max} - P_{\min})/\bar{P}]_2$	Dynamic $(\Delta \bar{P}_{rms}/\bar{P})_2$	Angular extent (below average), deg	Radial K_{ra}	Circumferential K_θ
A ^a	2.5 <										

^aNo bypass flow.^bOptimum centerbody bleed.

TABLE I. - Concluded. PERFORMANCE AND DISTORTION AT ANGLE-OF-ATTACK

(b) Supercritical terminal shock position

Configuration	Inlet Mach number, M_0	Centerbody bleed, m_{st}/m_o	Cowl bleed, m_{cb}/m_o	Performance		Distortion				
				Total pressure recovery, \bar{P}_2/P_0	Mass flow ratio, m_2/m_o	Angle-of-attack, α , deg	$[(P_{\max} - P_{\min})/P]^2$	Dynamic $(\Delta \bar{P}_{\text{rms}}/P)^2$	Angular extent (below average), deg	Radial K_{ra}
A ^a	2.5 <									

^aNo bypass flow.^bOptimum centerbody bleed.

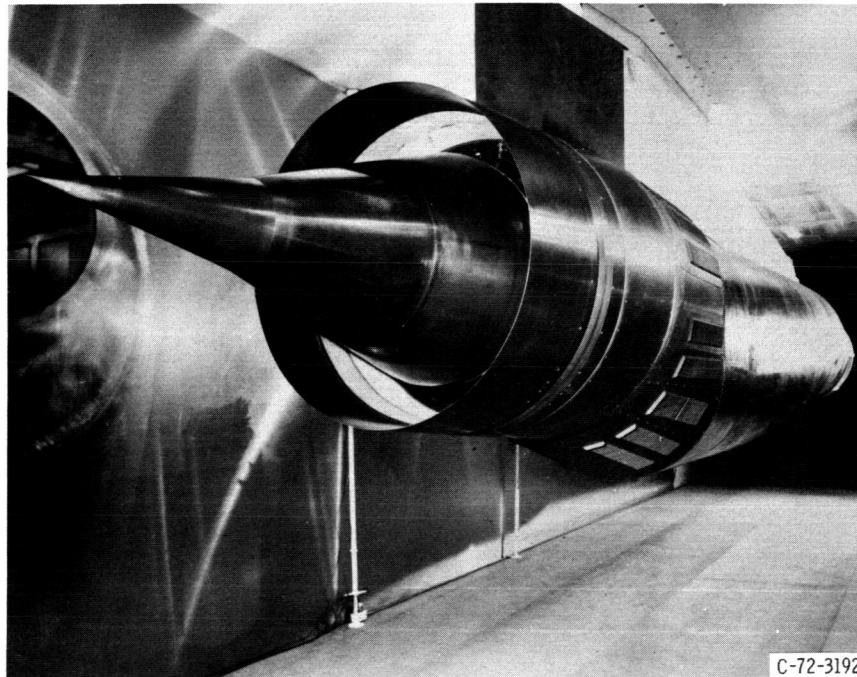


Figure 1. - Model installed in 10- by 10-Foot Supersonic Wind Tunnel.

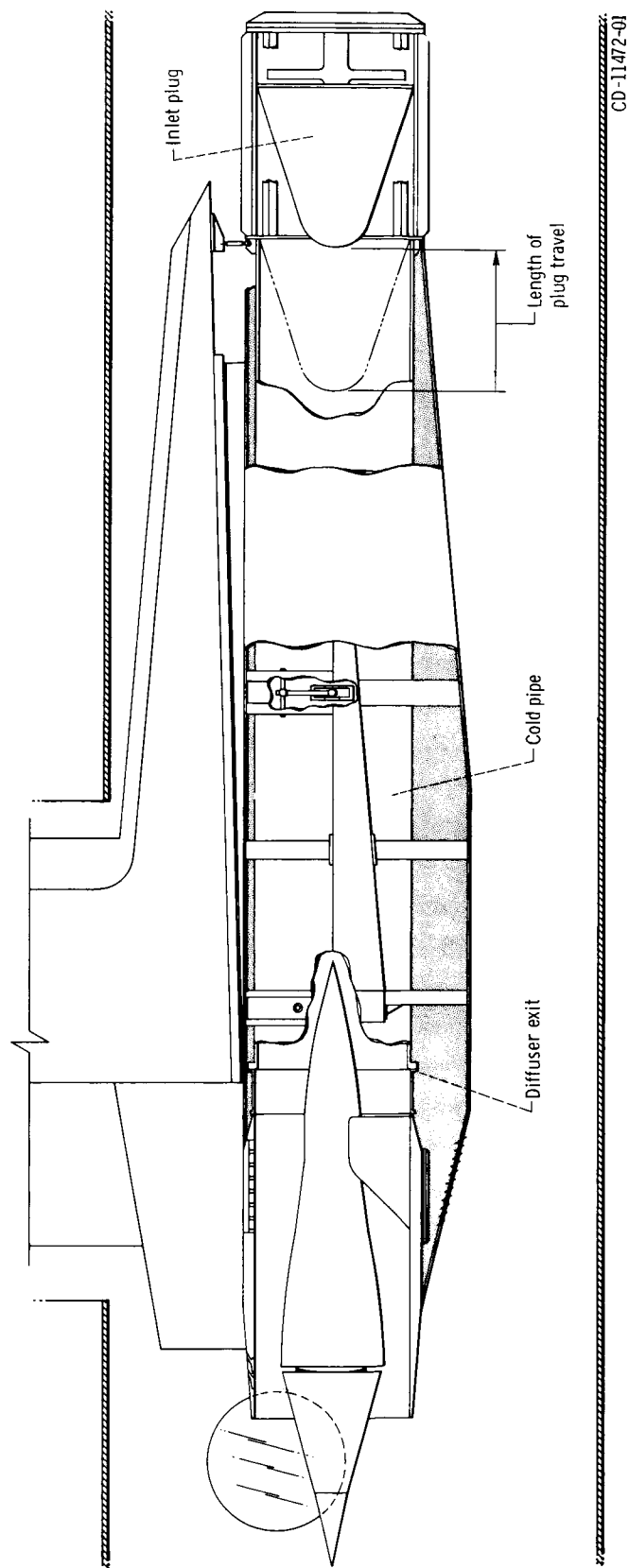
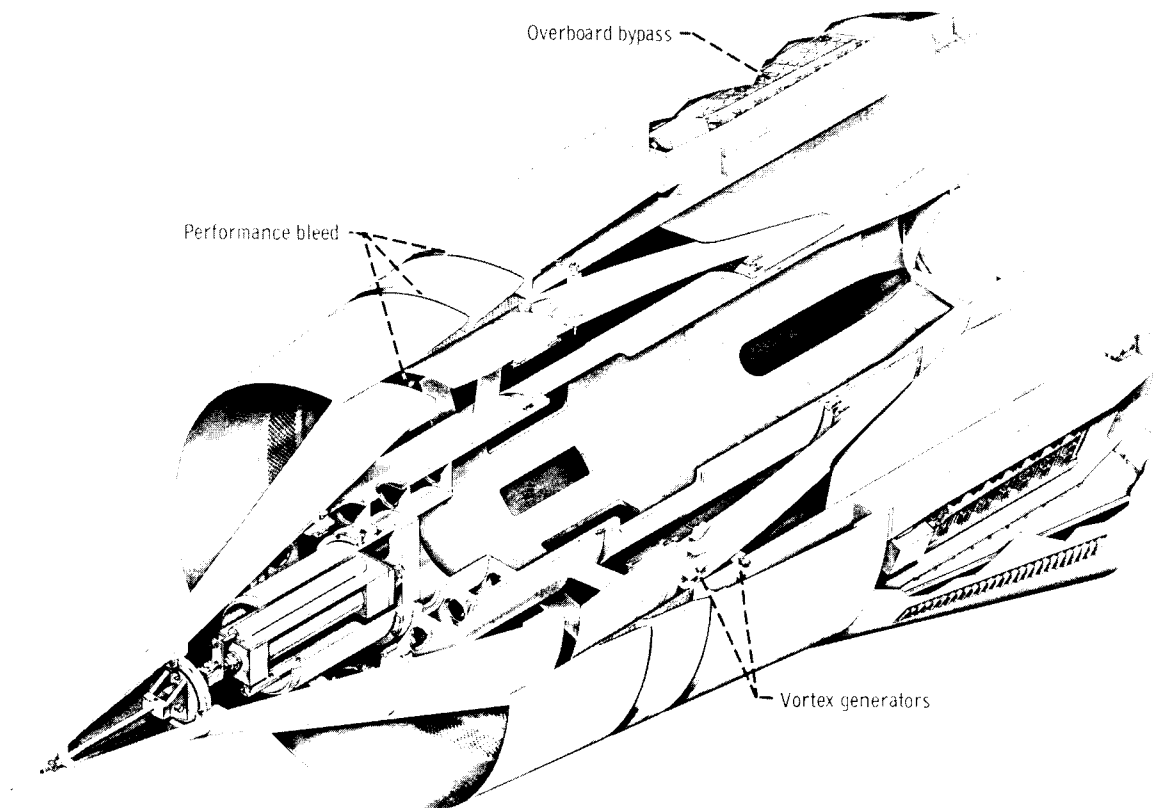


Figure 2. - Nacelle cutaway illustrating cold pipe installation.

CD-11472-Q1



CD-11556-01

Figure 3. - Isometric view of model details.

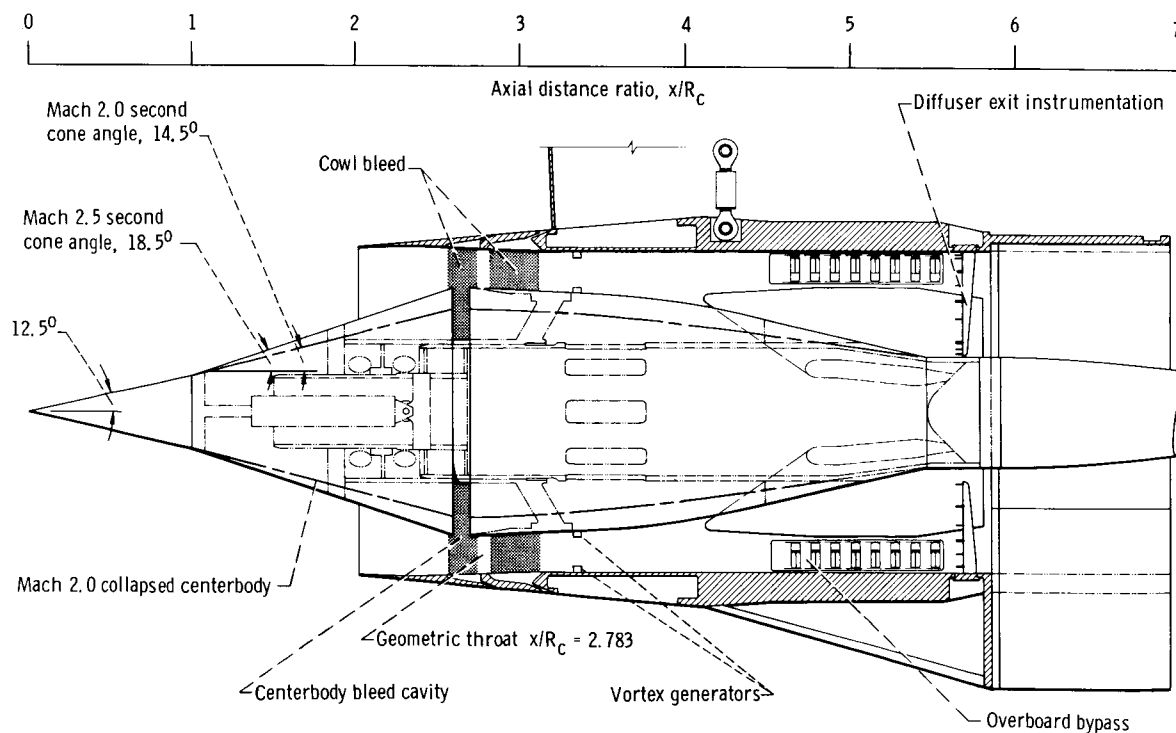


Figure 4. - Inlet cross section.

CD-11473-01

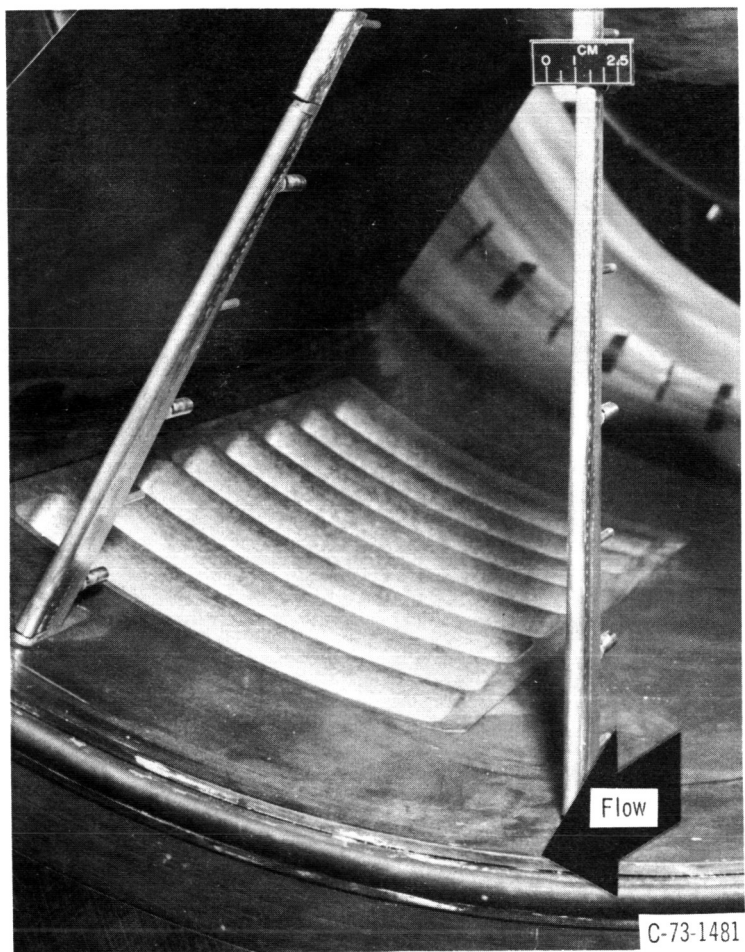


Figure 5. - Bypass entrance looking upstream from diffuser exit.

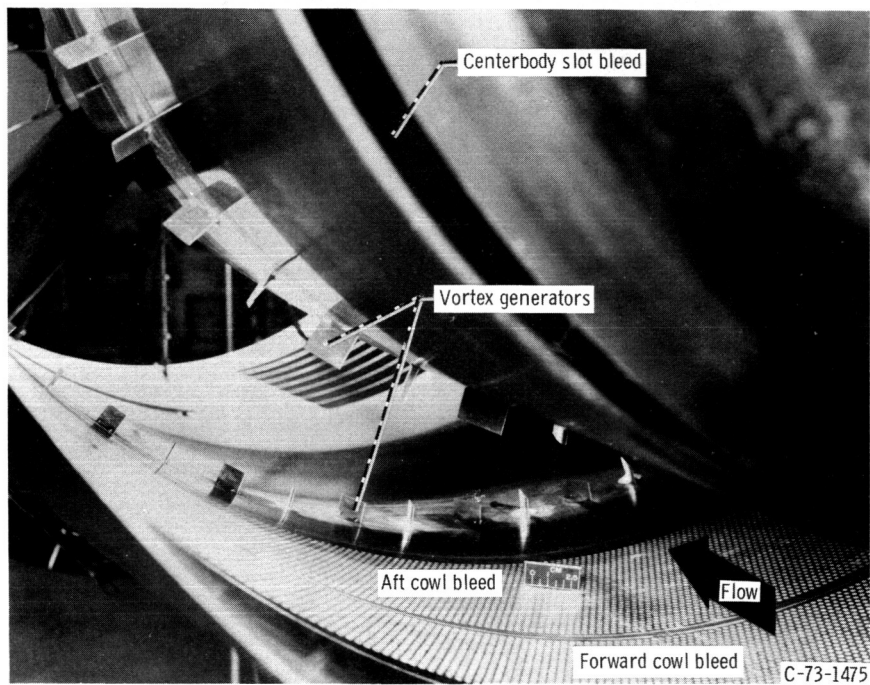

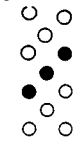


Figure 6. - Installation of vortex generators in inlet.

Cowl bleed configuration	Pattern	
	Forward	Aft
No cowl bleed	Sealed	Sealed
I	Rows 5 to 17 distributed as shown; ^a 0.012 supercritical bleed mass flow  Flow →	Rows 5 and 17 open
II	Same as configuration I except 0.021 supercritical bleed mass flow	Rows 5 and 17 open
III	Rows 1 to 25 as shown ^a  Flow →	Sealed
IV	Rows 12 and 13 open	Rows 5 and 17 open

^aOpen symbols denote sealed holes; solid symbols denote open holes.

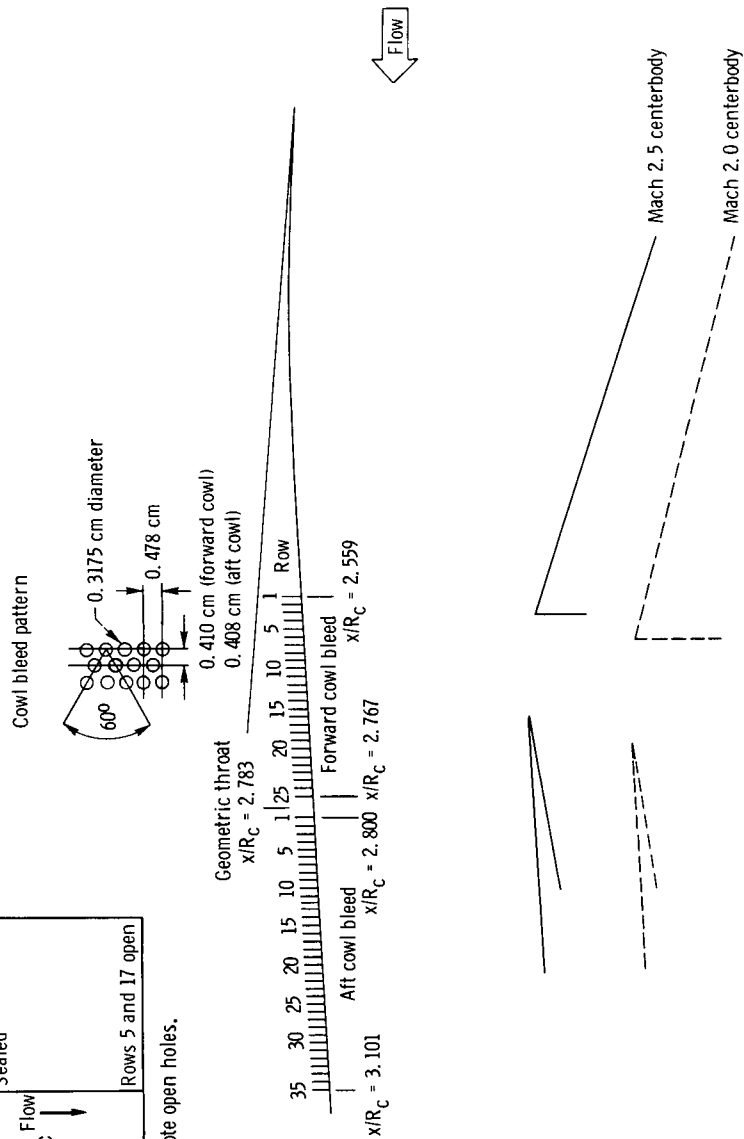
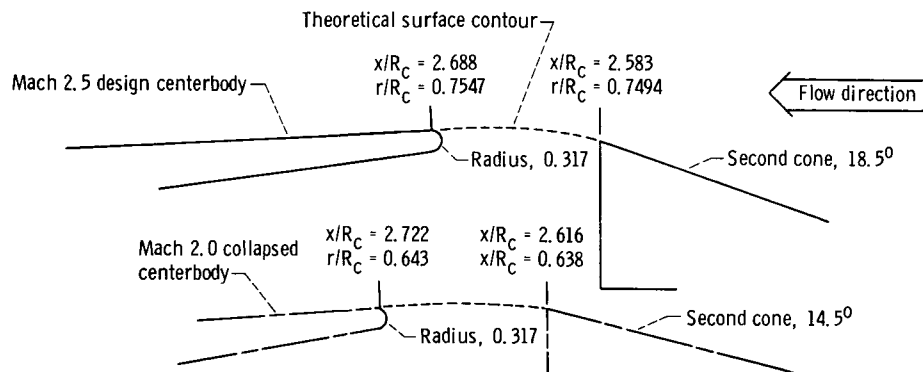
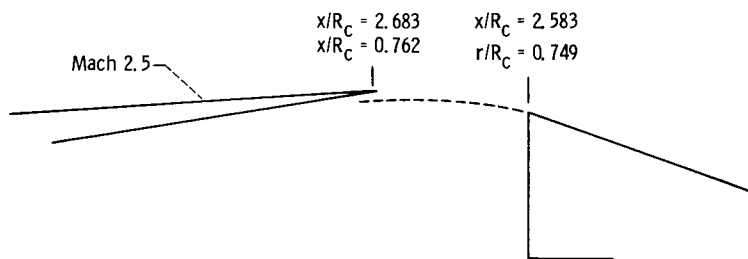


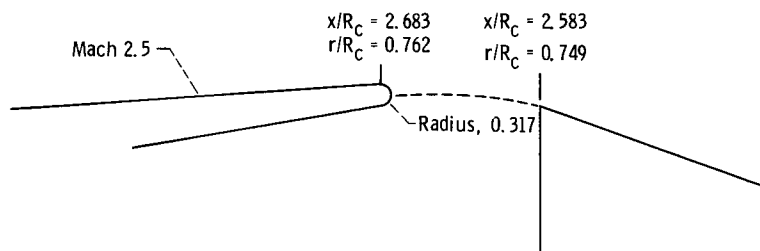
Figure 7. - Cowl performance bleed configuration.



(a) Configuration A; blunt lip, flush slot.

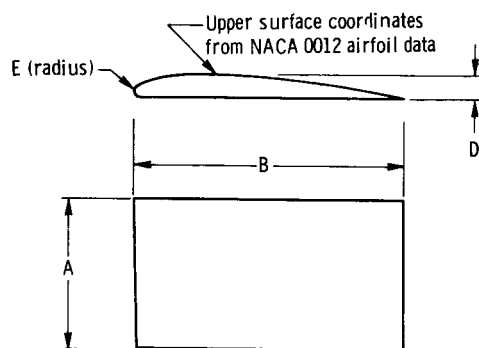


(b) Configuration B; sharp lip, ram scoop.



(c) Configuration C; blunt lip, ram scoop.

Figure 8. - Centerbody bleed configurations. (All dimensions in cm.)



Location	Dimensions, cm				
	A	B	C	D	E
Cowl	1.52	3.028	4.839	0.183	0.030
Centerbody	2.03	4.036	4.864	.244	.041

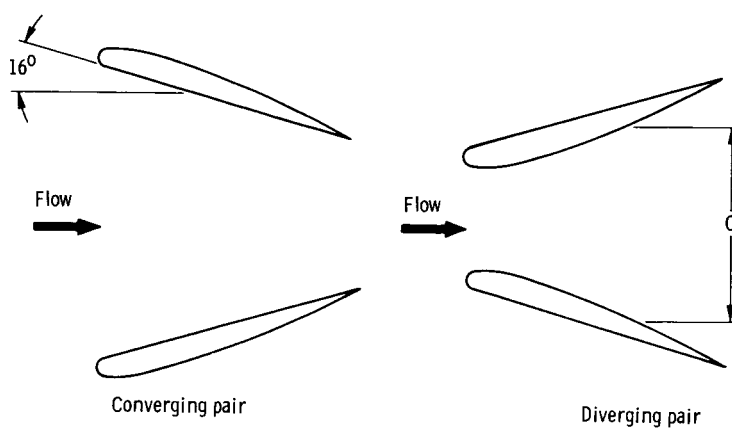


Figure 9. - Vortex generator details.

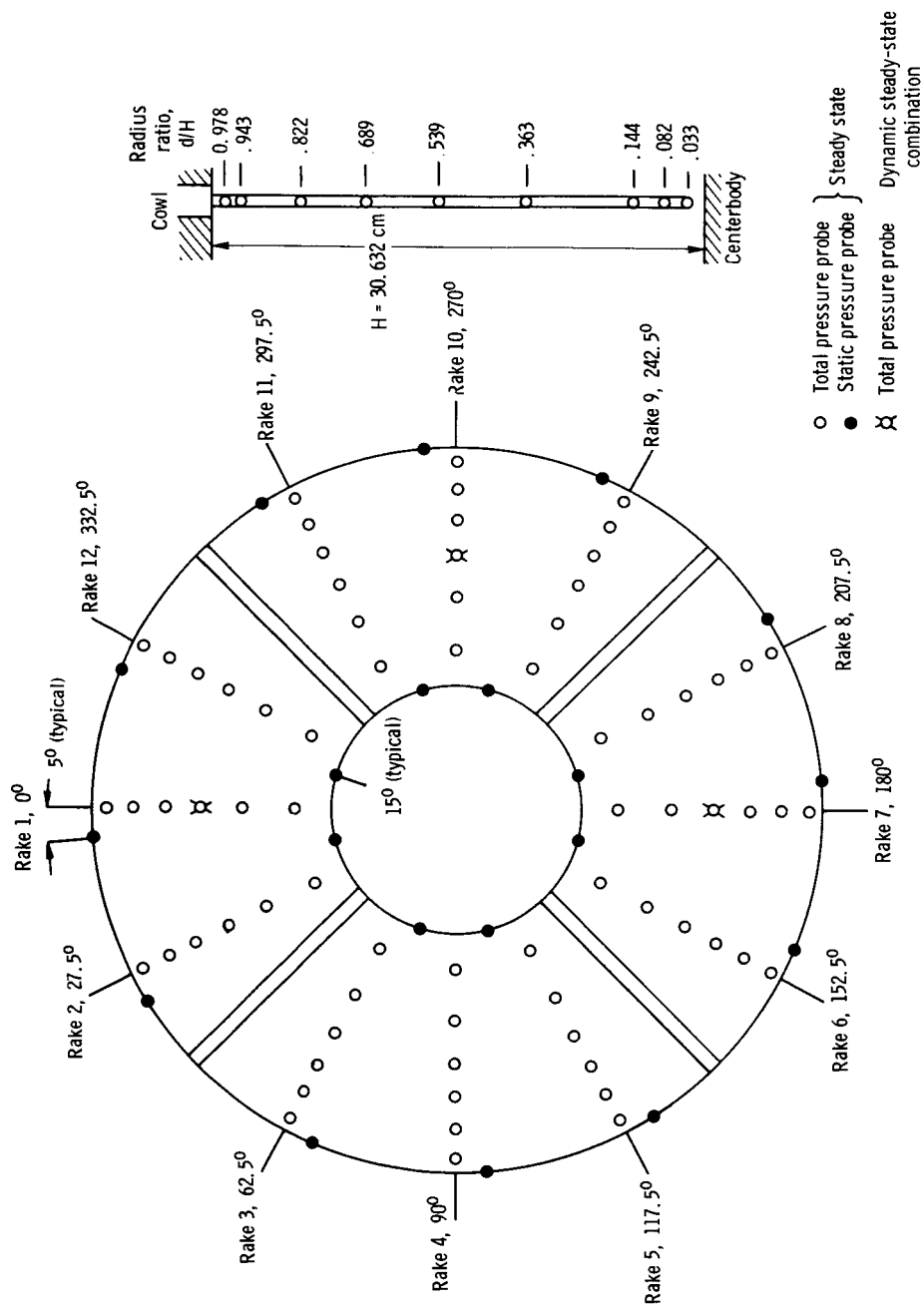


Figure 10. - Diffuser exit pressure instrumentation looking downstream.

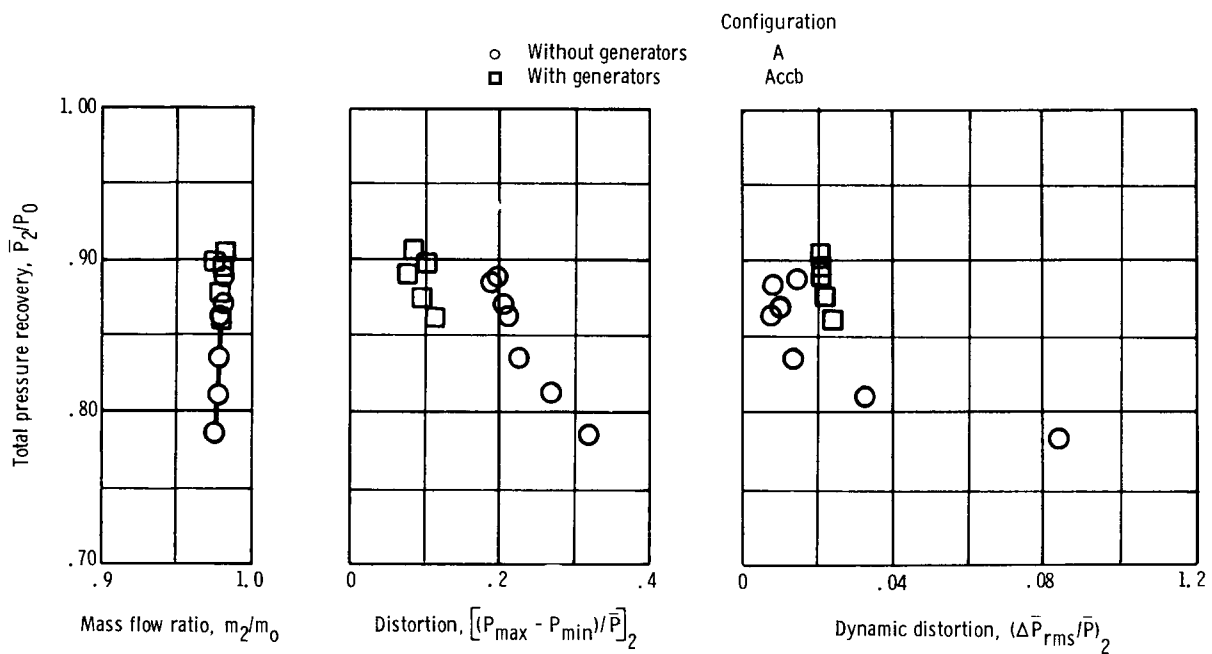


Figure 11. - Effect of vortex generators on steady-state and dynamic inlet performance. Angle-of-attack, 0° ; inlet Mach number, 2.5; cowl-lip position parameter, 26.4° ; no bypass flow.

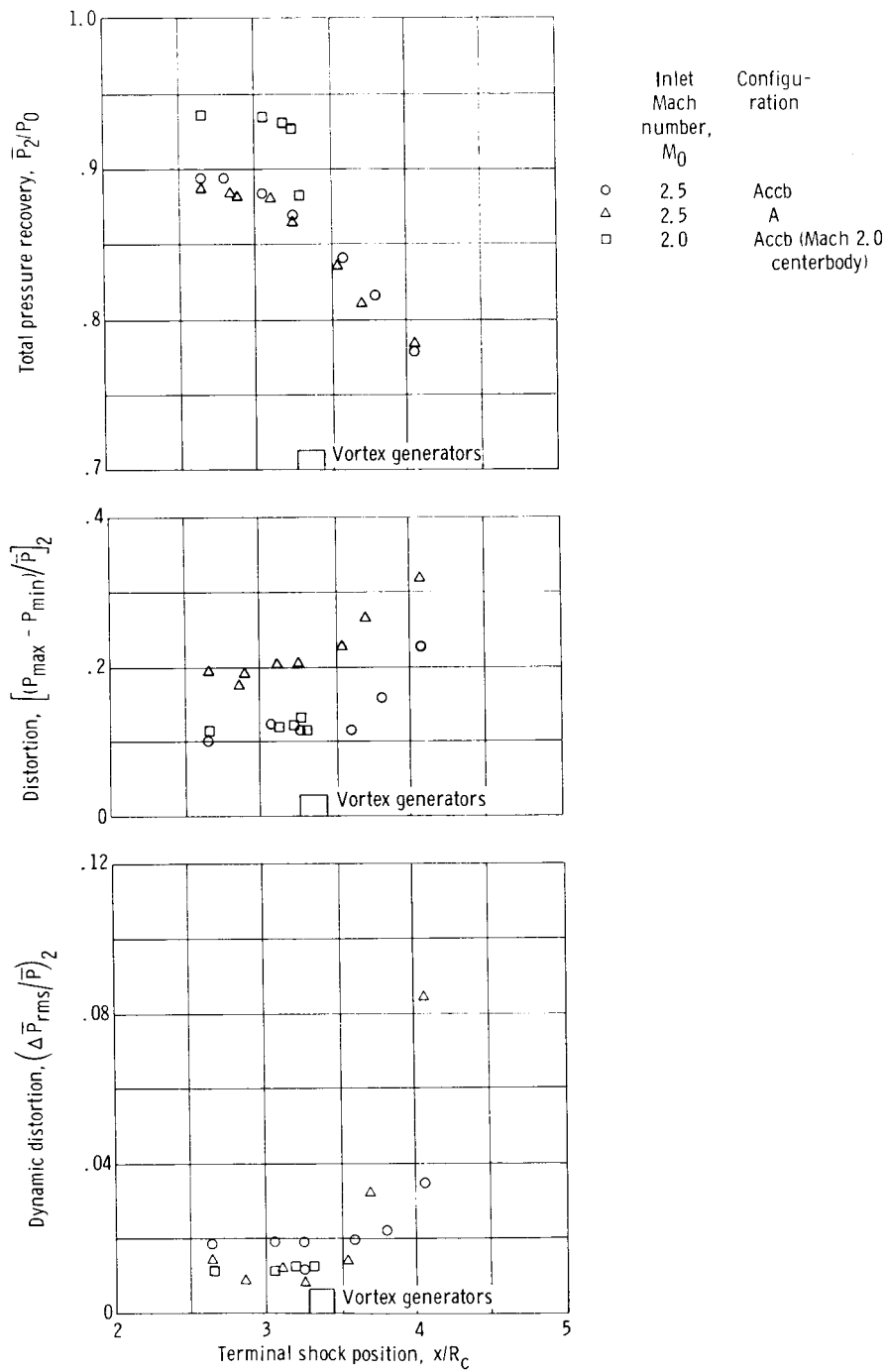


Figure 12. - Variation of steady-state and dynamic inlet performance with terminal shock position. Exit plug variation; angle-of-attack, 0° ; lip-position parameter, 26.4° .

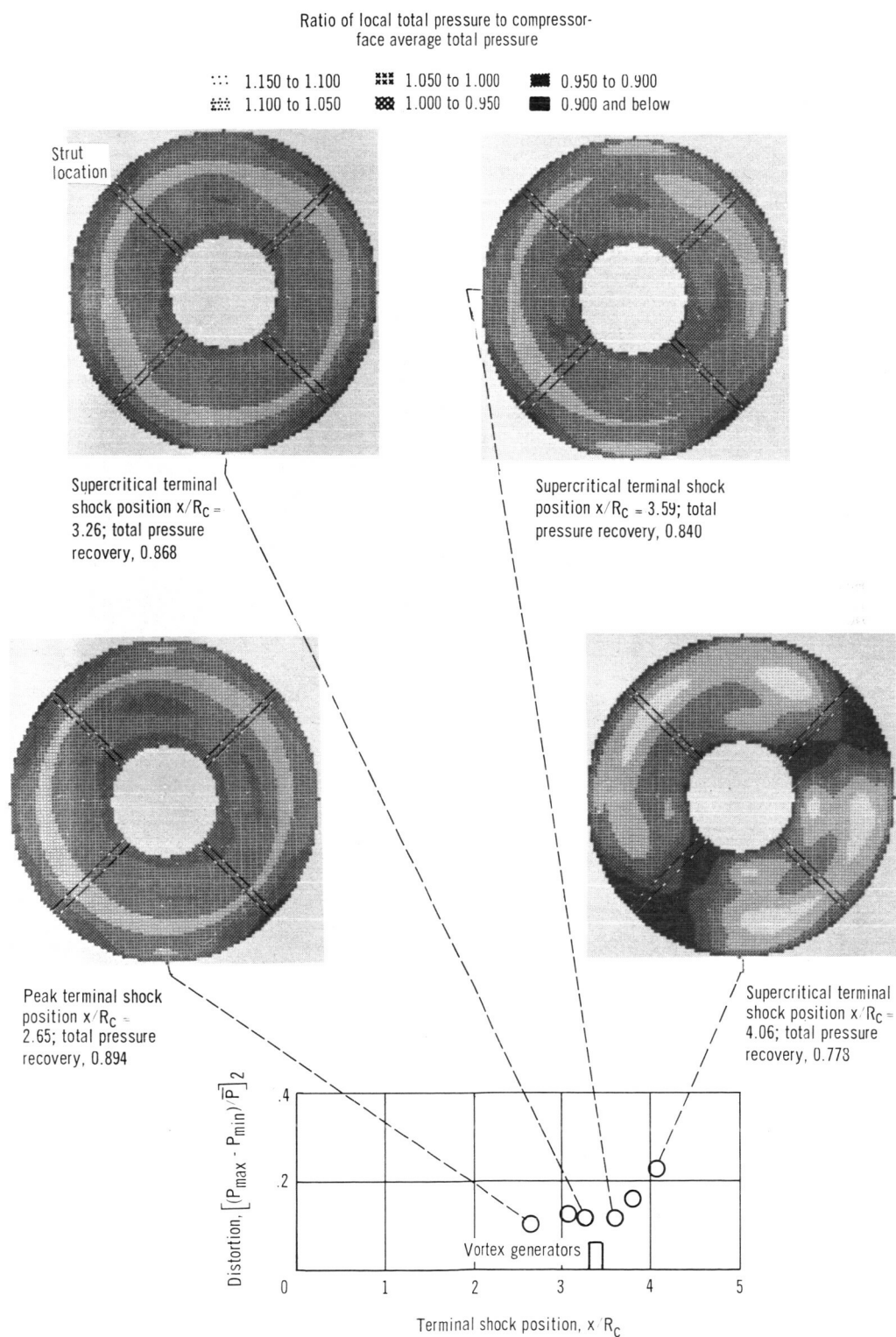
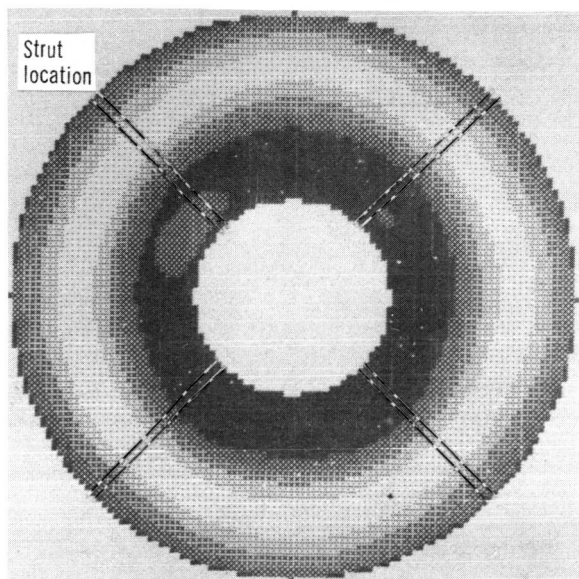


Figure 13. - Steady-state distortion contours at diffuser exit. Configuration Accb; exit plug variation; angle-of-attack, 0° ; inlet Mach number, 2.5; cowl-lip-position parameter, 26.4° .

Ratio of local total pressure to compressor-face average total pressure

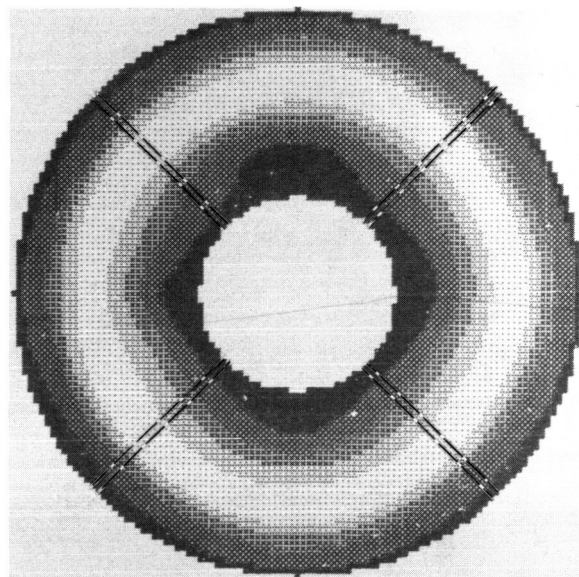
::: 1.150 to 1.100	1.000 to 0.950
::: 1.100 to 1.050	0.950 to 0.900
::: 1.050 to 1.000	0.900 and below



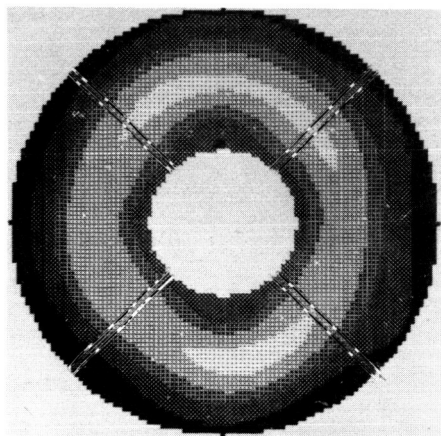
(a) Peak terminal shock position. Total pressure recovery, 0.888.

Ratio of local total pressure to compressor-face average total pressure

::: 1.150 to 1.100	1.000 to 0.950
::: 1.100 to 1.050	0.950 to 0.900
::: 1.050 to 1.000	0.900 and below



(b) Critical terminal shock position. Total pressure recovery, 0.886.

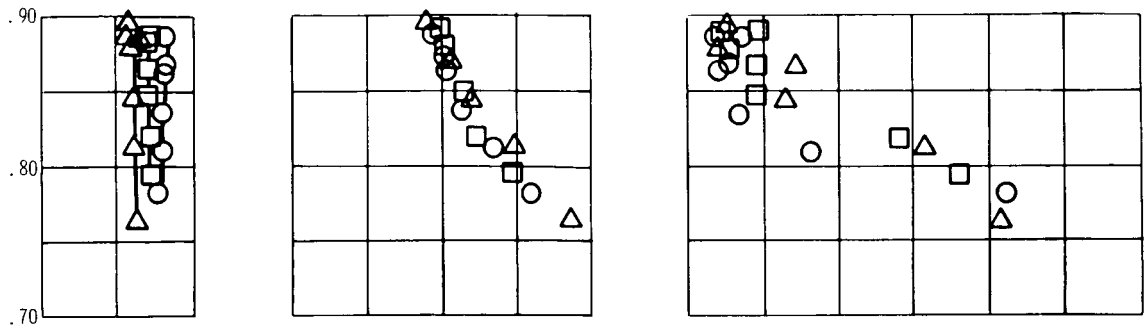


Ratio of local total pressure to compressor-face average total pressure

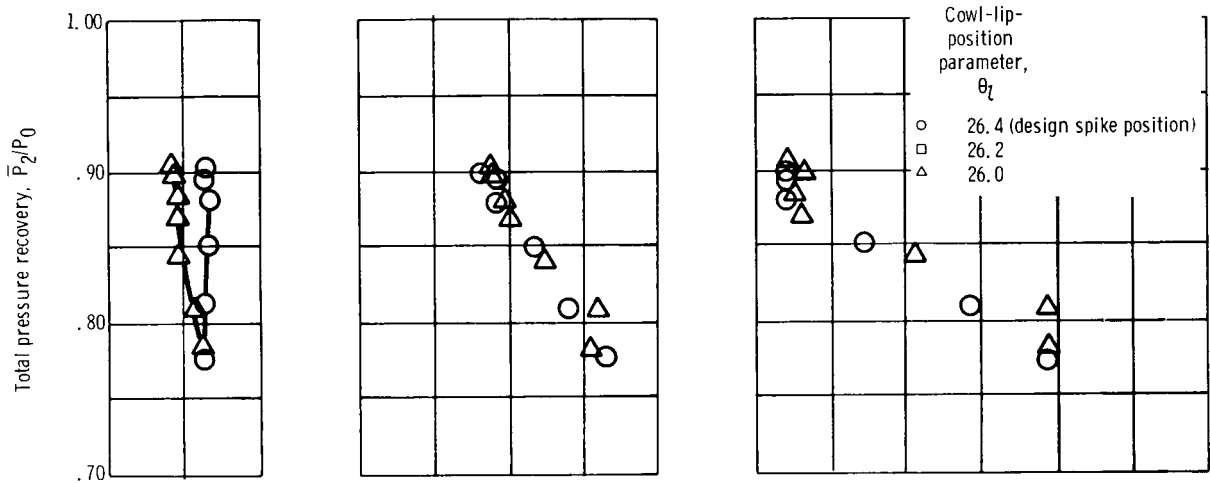
::: 1.300 to 1.200	1.000 to 0.900
::: 1.200 to 1.100	0.900 to 0.800
::: 1.100 to 1.000	0.800 and below

(c) Supercritical terminal shock position. Total pressure recovery, 0.784.

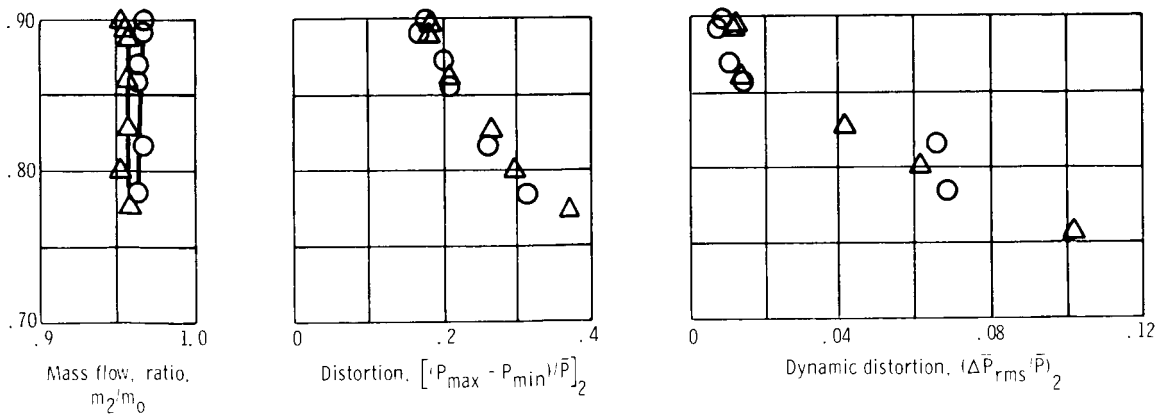
Figure 14. - Steady-state distortion contours at diffuser exit. Configuration A; free-stream Mach number, 2.5; cowl-lip-position parameter, 26.4°.



(a) Configuration A.



(b) Configuration B.



(c) Configuration C.

Figure 15. - Effect of centerbody bleed and spike position on steady-state and dynamic inlet performance. Angle-of-attack, 0° ; inlet Mach number, 2.5; no bypass flow.

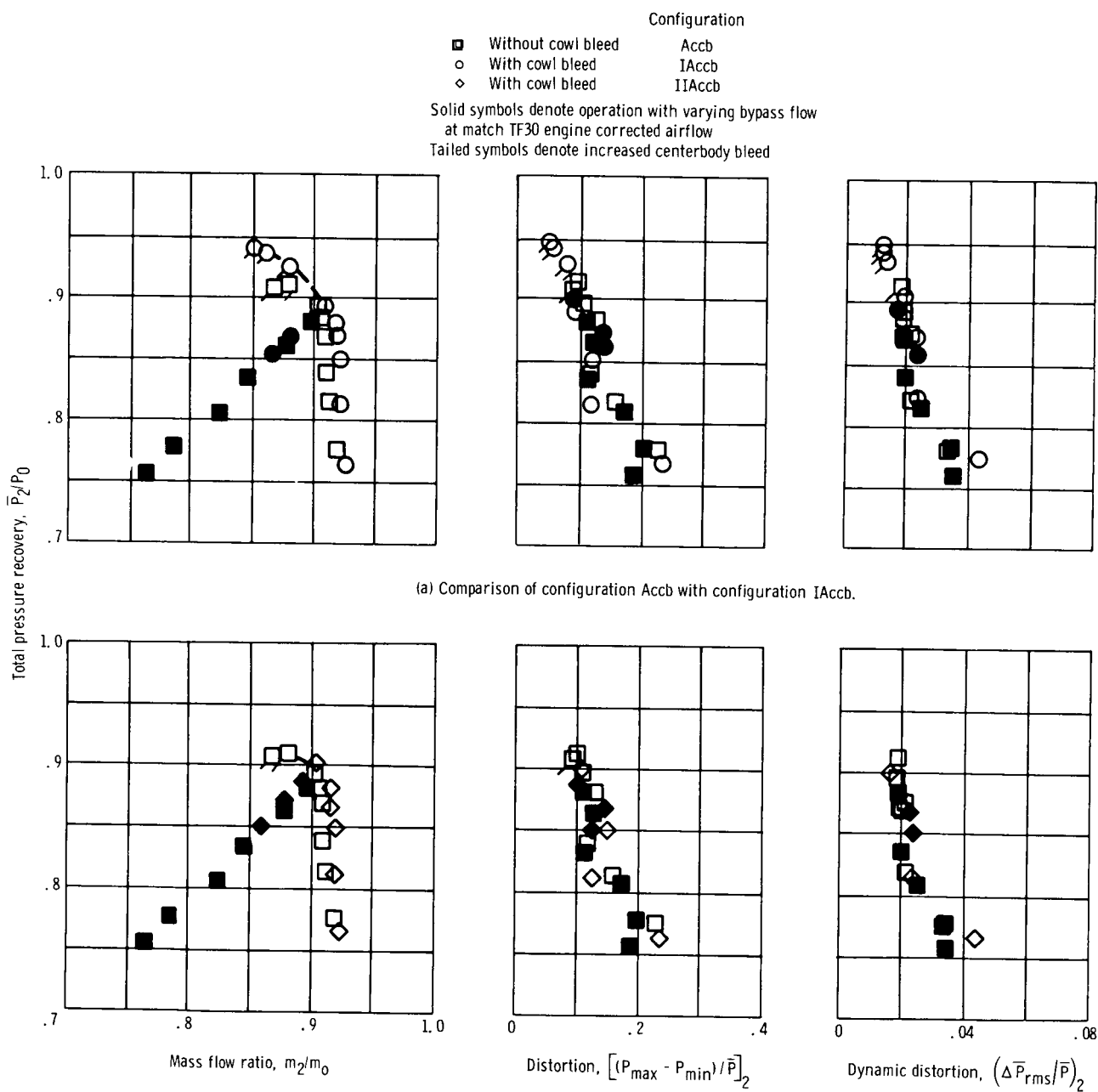
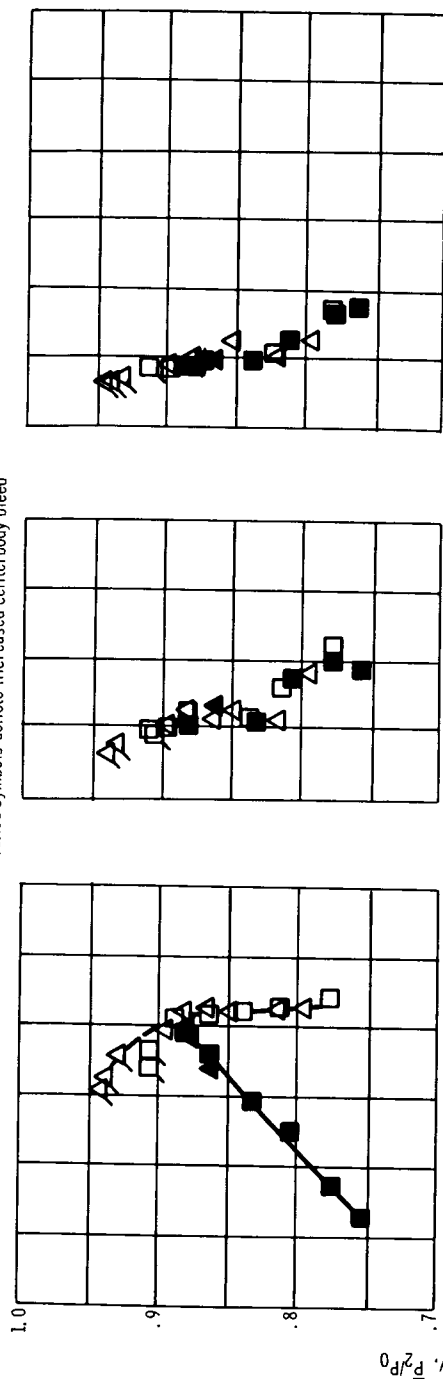


Figure 16. - Effect of cowl bleed on steady-state and dynamic inlet performance. Angle-of-attack, 0° ; inlet Mach number, 2.5; cowl-lip position parameter, 26.4° .

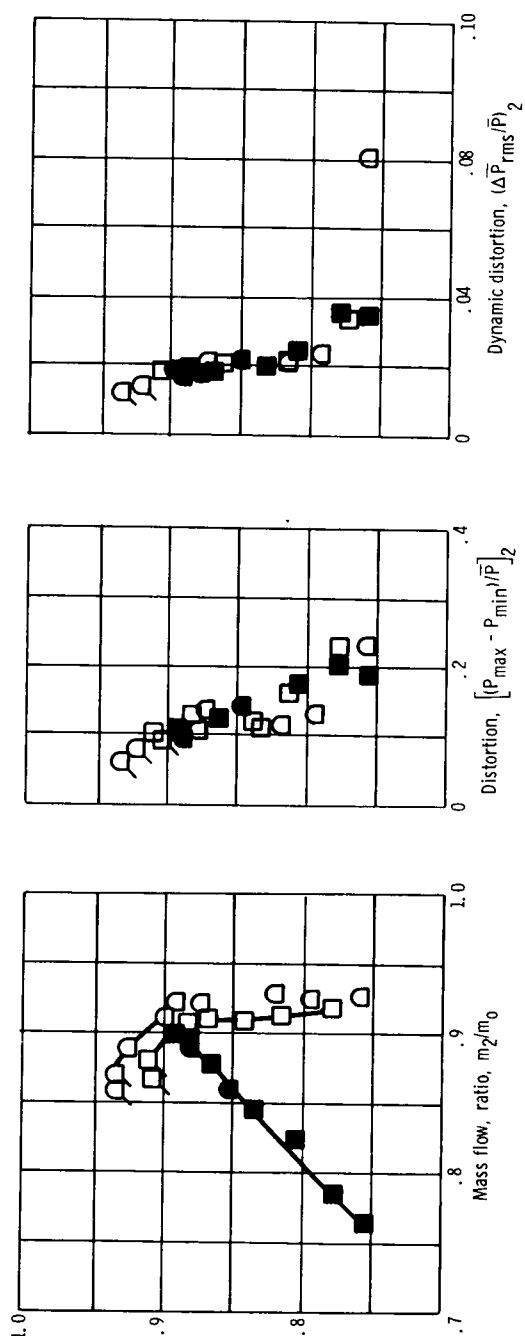
Configuration

- Without cowl bleed
- △ With cowl bleed
- IIIIAcCb
- IVAcCb

Solid symbols denote operation with varying bypass flow at match TF30 engine corrected airflow
 Tailed symbols denote increased centerbody bleed



(c) Comparison of configuration AcCb with configuration IIIIAcCb.



(d) Comparison of configuration AcCb with configuration IVAcCb.

Figure 16. - Concluded.

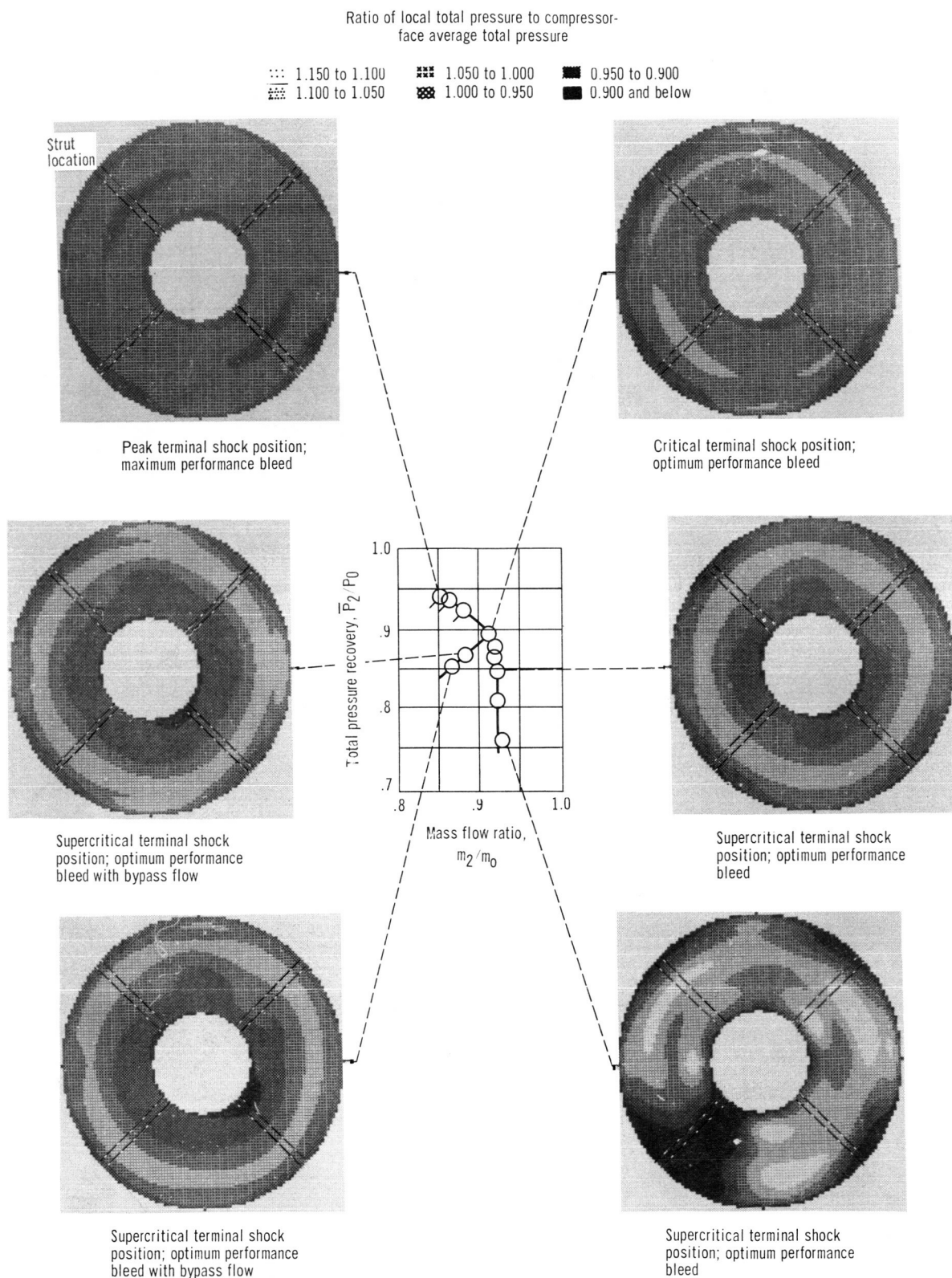


Figure 17. - Steady-state distortion patterns at diffuser exit. Configuration IACcb; inlet Mach number, 2.5; angle-of-attack, 0° ; cowl-lip-position parameter, 26.4° .

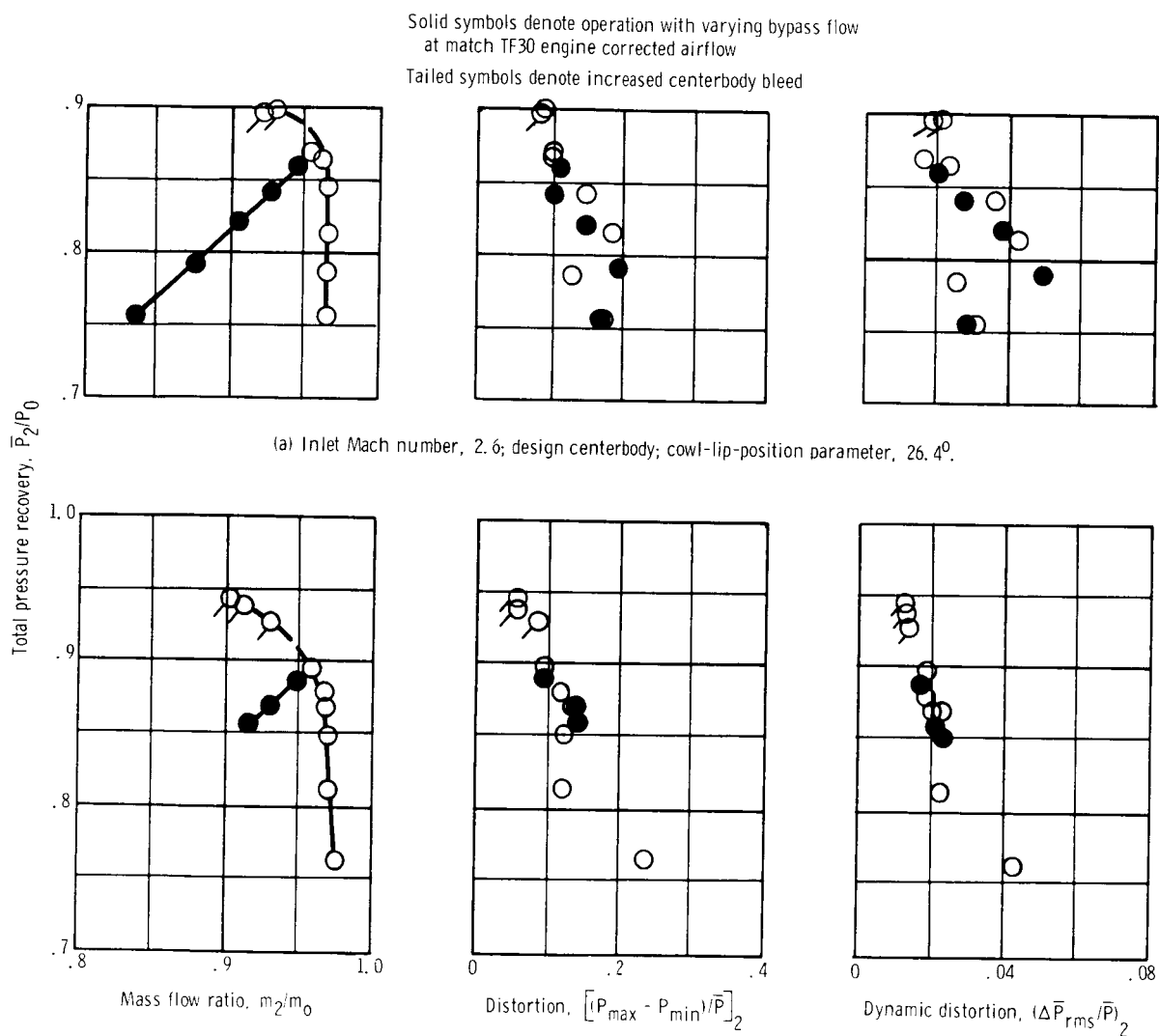
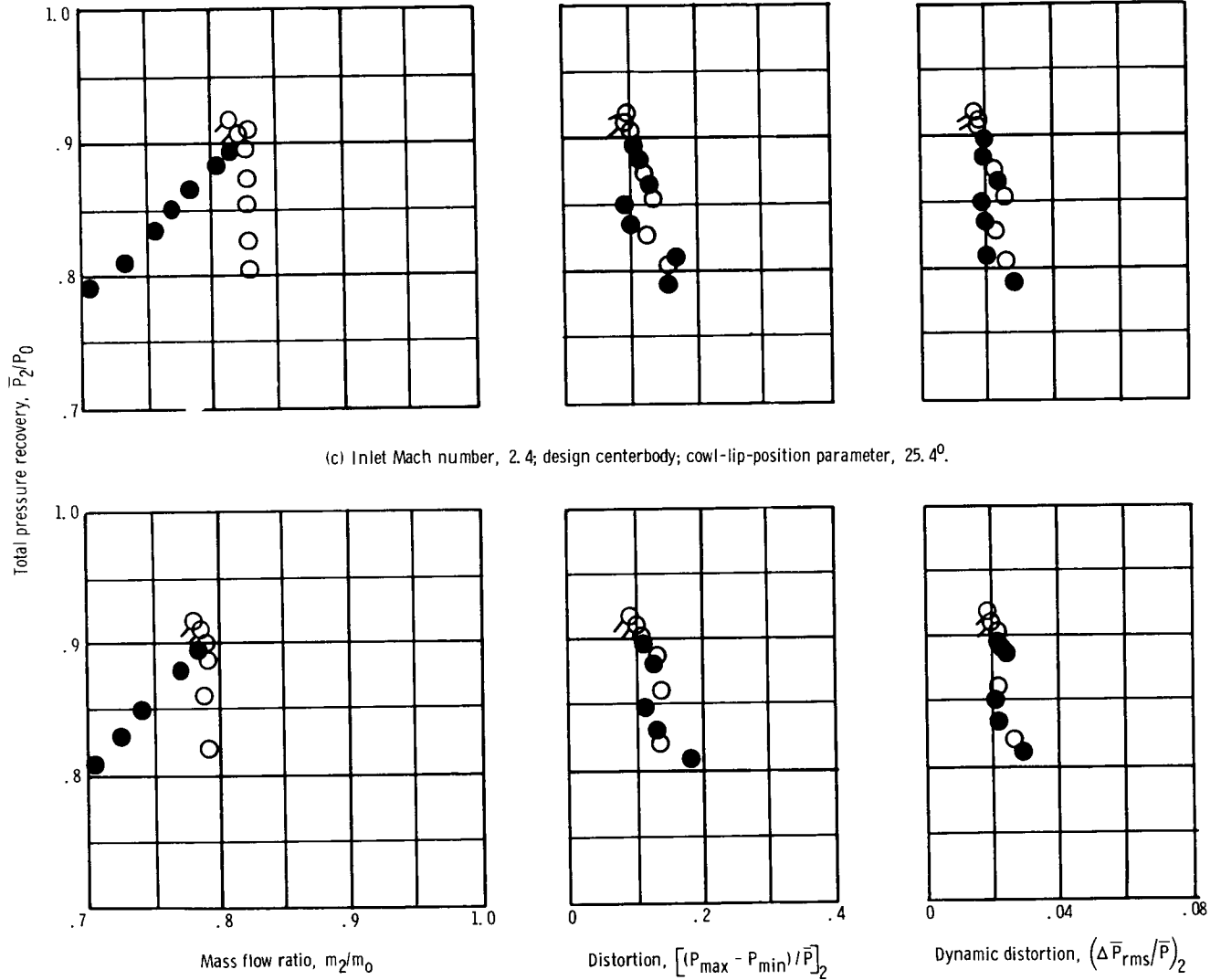


Figure 18. - Effect of inlet Mach number on steady-state and dynamic inlet performance. Configuration TAccb; angle of attack, 0°.

Solid symbols denote operation with varying bypass
flow at match TF30 engine corrected airflow
Tailed symbols denote increased centerbody bleed



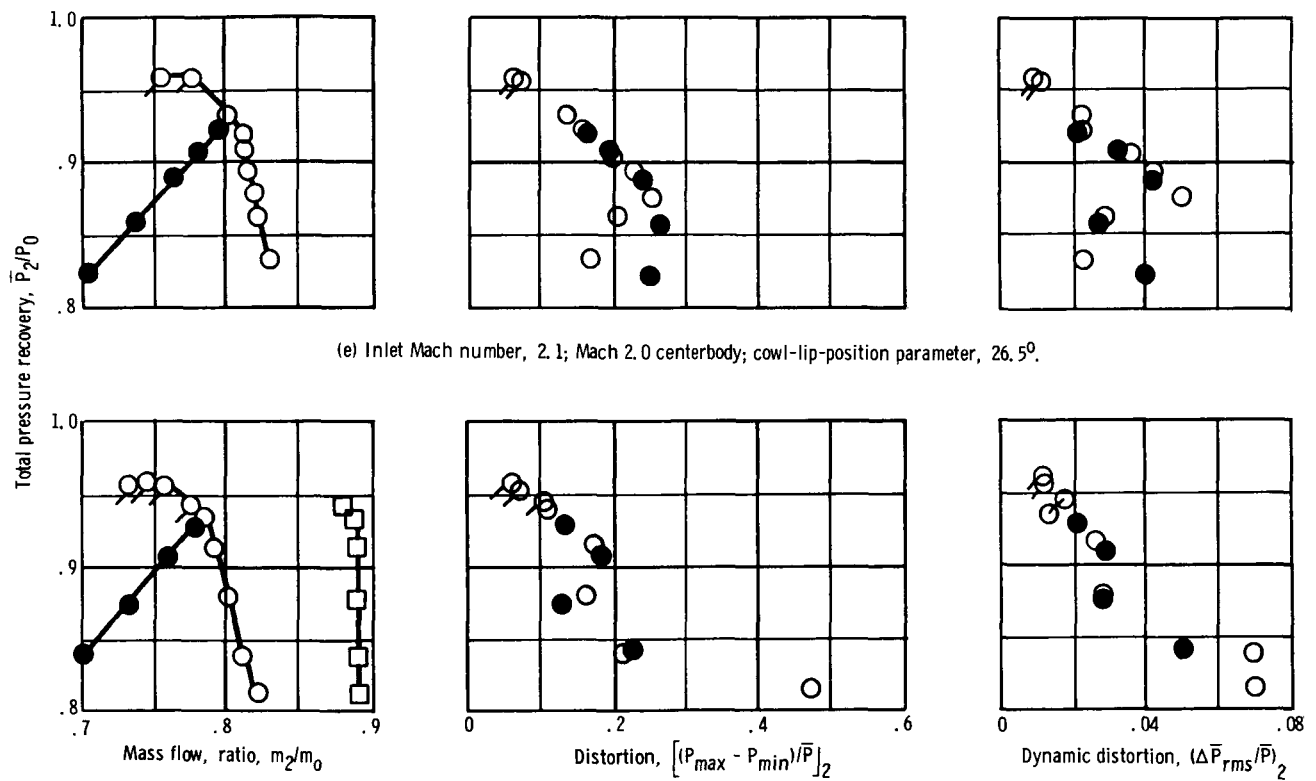
(c) Inlet Mach number, 2.4; design centerbody; cowl-lip-position parameter, 25.4°.

(d) Inlet Mach number, 2.3; design centerbody; cowl-lip-position parameter, 24.9°.

Figure 18. - Continued.

- Mass flow ratio plus bypass flow ratio
 $(m_2 + m_{by})/m_0$
- Mass flow ratio m_2/m_0

Solid symbols denote operation with varying bypass flow
 at match TF30 engine corrected airflow
 Tailed symbols denote increased centerbody bleed



(e) Inlet Mach number, 2.1; Mach 2.0 centerbody; cowl-lip-position parameter, 26.5°.

(f) Inlet Mach number, 2.0; Mach 2.0 centerbody; cowl-lip-position parameter, 26.4°.

Figure 18. - Concluded.

Ratio of local total pressure to compressor-face average total pressure

1.150 to 1.100

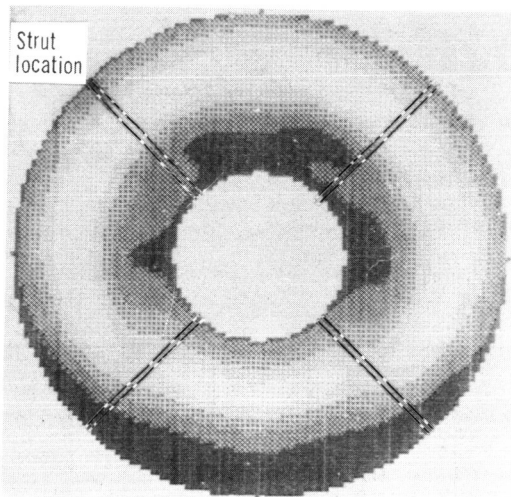
1.050 to 1.000

0.950 to 0.900

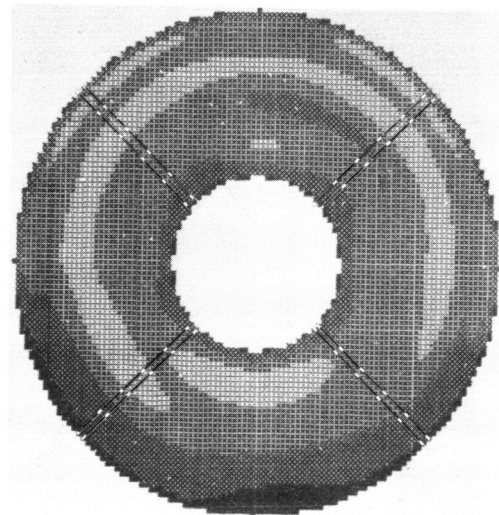
1.100 to 1.050

1.000 to 0.950

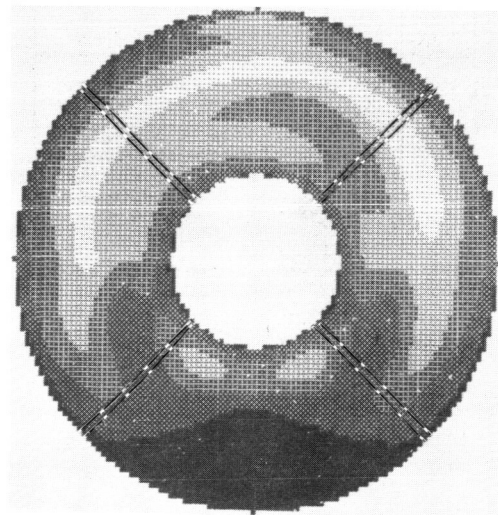
0.900 and below



(a) Critical terminal shock position. Configuration A; angle-of-attack, 1.85° ; total pressure recovery, 0.881; mass flow ratio, 0.963; circumferential distortion index, 0.550.



(b) Critical terminal shock position. Configuration Accb; angle-of-attack, 2.16° ; total pressure recovery, 0.891; mass flow ratio, 0.972; circumferential distortion index, 0.295.



(c) Critical terminal shock position. Configuration Accb; angle-of-attack, 4.17° ; total pressure recovery, 0.857; mass flow ratio, 0.861; circumferential distortion index, 0.457.

Figure 19. - Diffuser exit steady-state total pressure contours. Inlet Mach number, 2.495; cowl-lip-position parameter, 26.4° .

Ratio of local total pressure to compressor-face average total pressure

::: 1.300 to 1.200

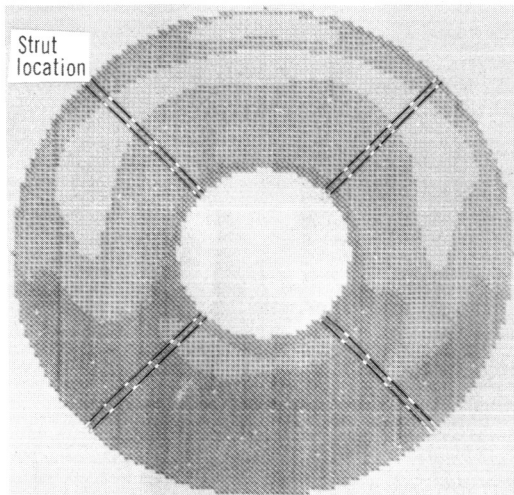
xxx 1.100 to 1.000

■ 0.900 to 0.800

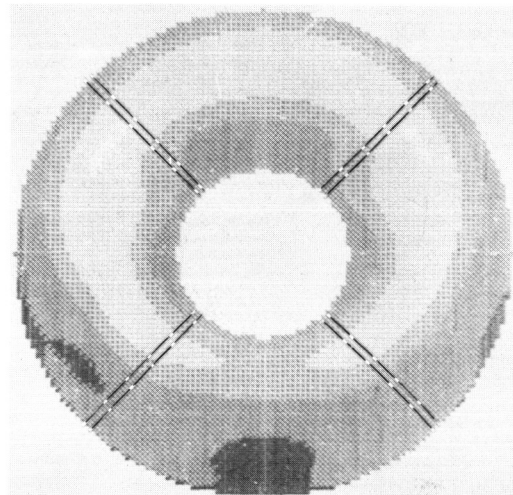
xxx 1.200 to 1.100

xxx 1.000 to 0.900

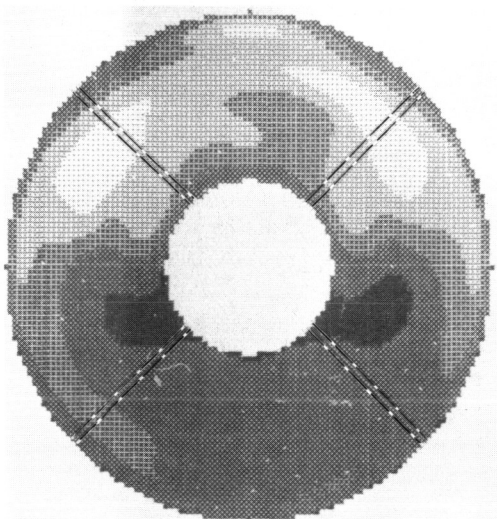
■ 0.800 and below



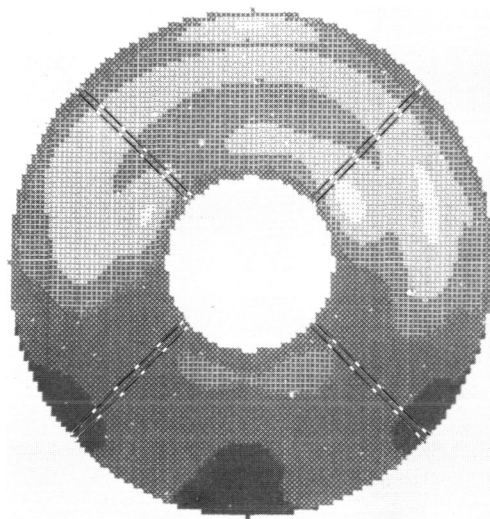
(d) Critical terminal shock position. Configuration IIACcb; angle-of-attack, 7.19° ; total pressure recovery, 0.840; mass flow ratio, 0.842; circumferential distortion index, 0.635.



(e) Supercritical terminal shock position. Configuration A; angle-of-attack, 3.40° ; total pressure recovery, 0.843; mass flow ratio, 0.947; circumferential distortion index, 0.632.

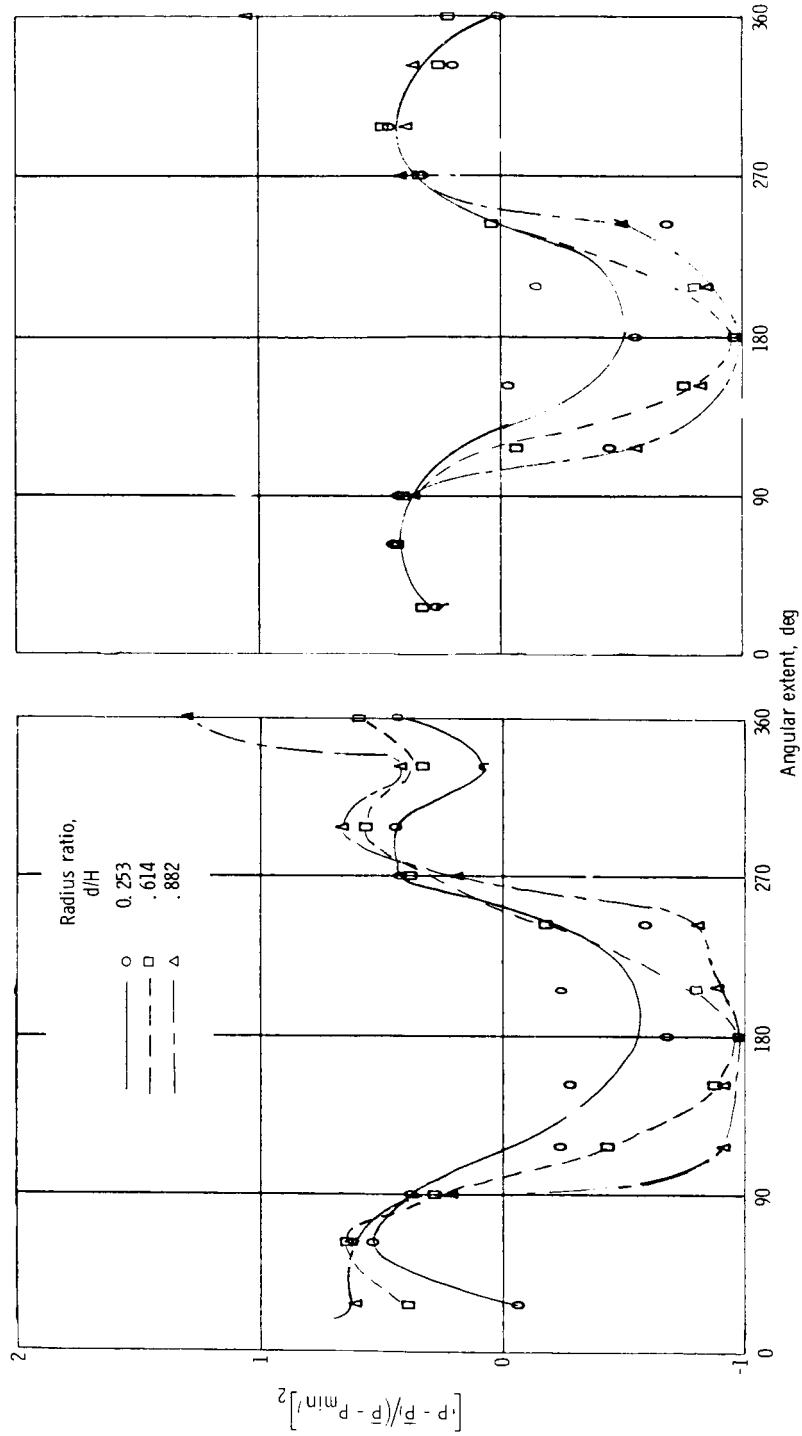


(f) Supercritical terminal shock position. Configuration IIACcb; angle-of-attack (strut limitation), 7.96° ; total pressure recovery, 0.739; mass flow ratio, 0.857; circumferential distortion index, 0.746.



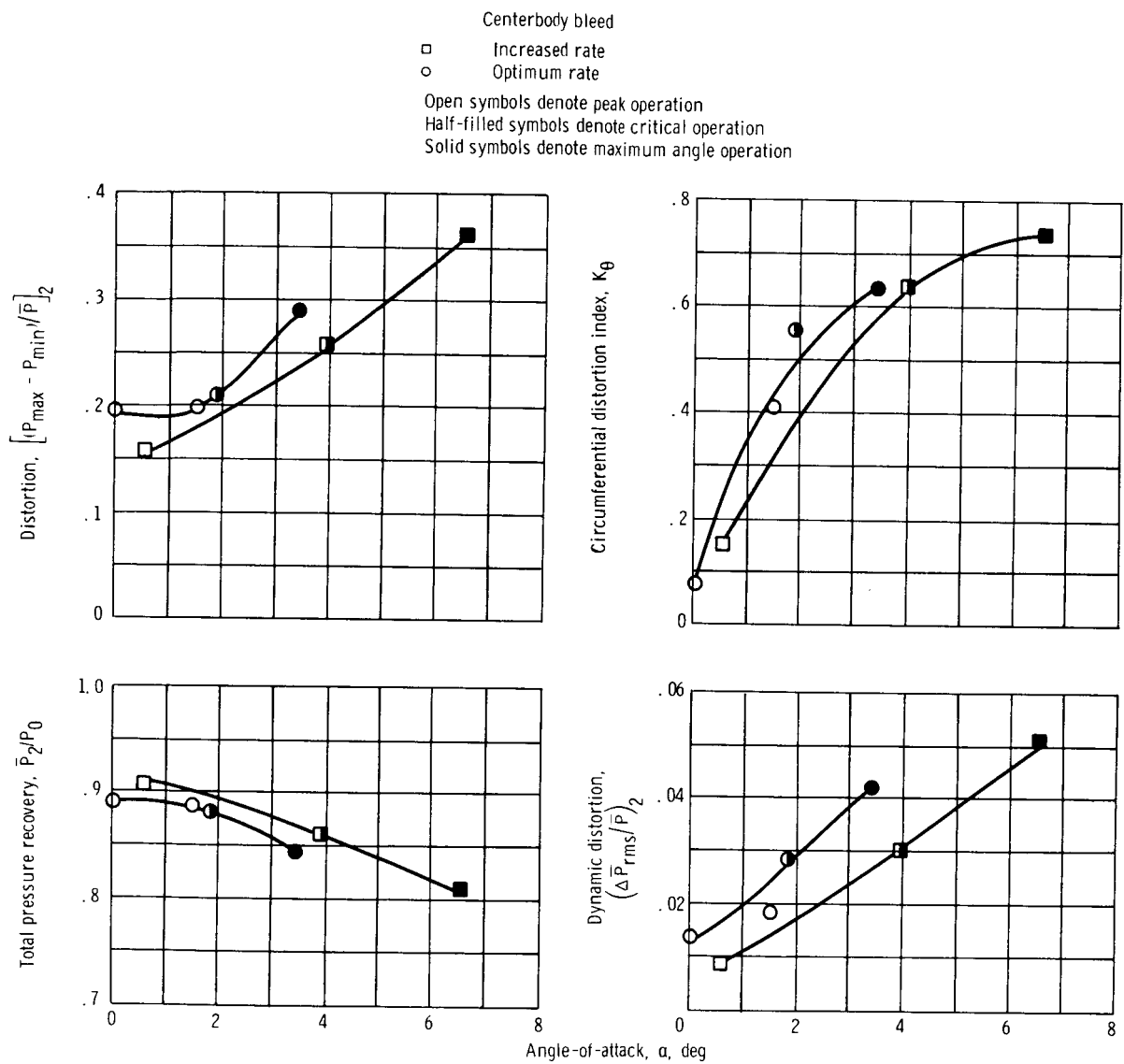
(g) Supercritical terminal shock position. Configuration Accb; angle-of-attack, 6.84° ; total pressure recovery, 0.781; mass flow ratio, 0.850; circumferential distortion index, 0.721.

Figure 19. - Concluded.



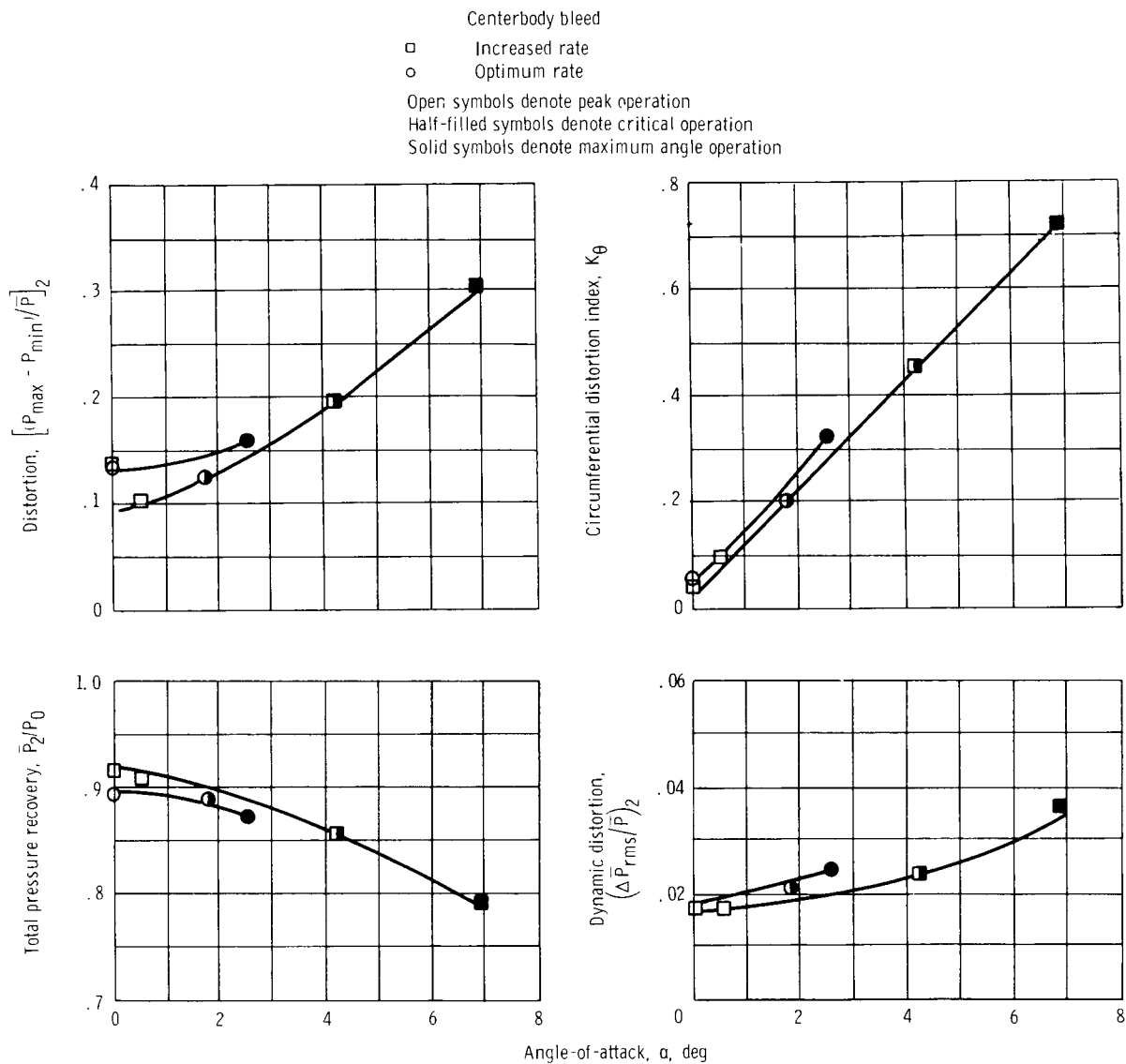
(a) Critical inlet operation. Angle-of-attack, 6.83°; centerbody bleed flow, 0.045; total pressure recovery, 0.843. (b) Supercritical inlet operation. Angle-of-attack, 4.96°; centerbody bleed flow, 0.022; total pressure recovery, 0.840.

Figure 20. - Angular extent of distortion at diffuser exit. Configuration IAccb; inlet Mach number, 2.5; cowl-lip-position parameter, 26.4°.



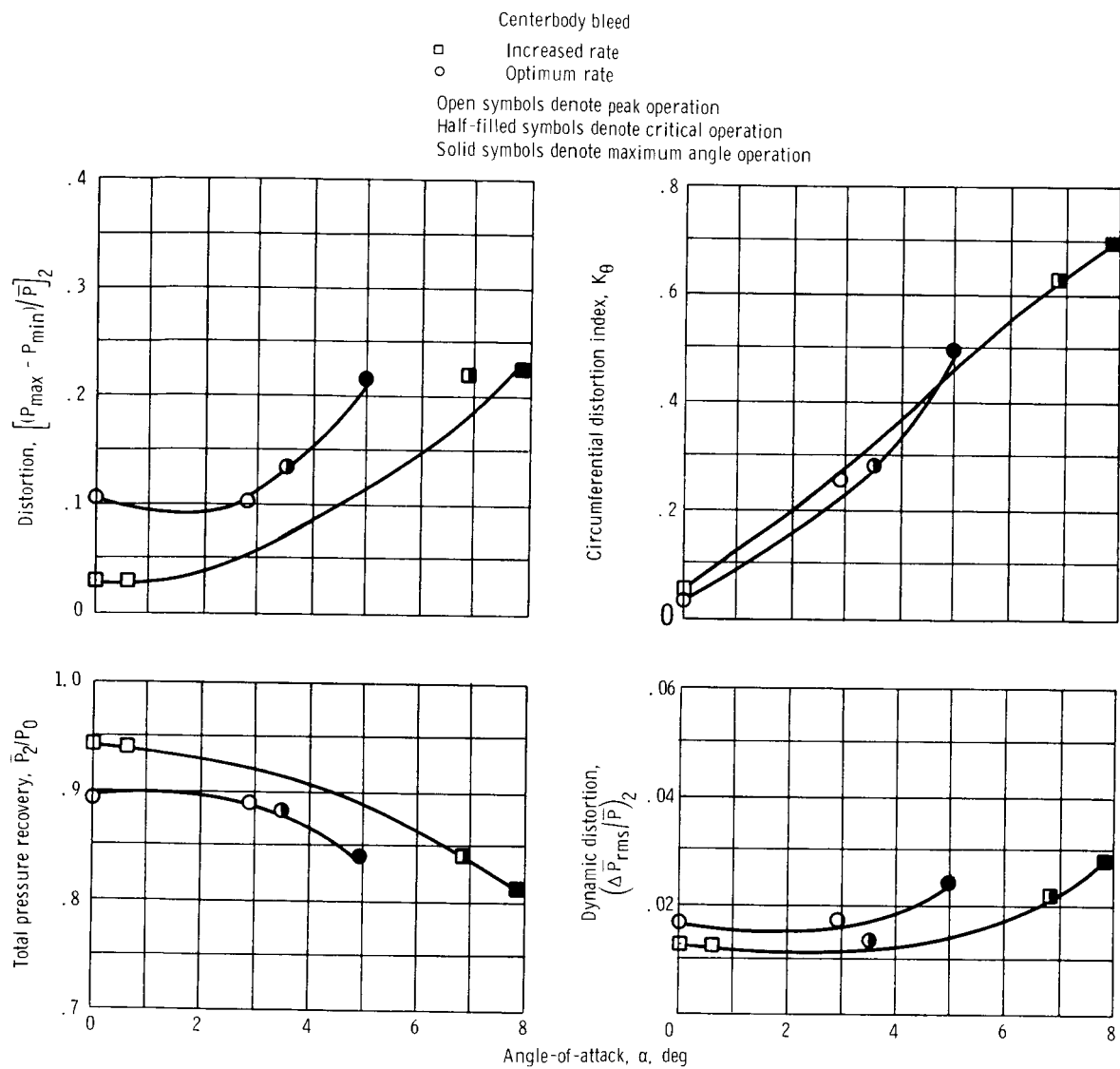
(a) Inlet Mach number, 2.5; configuration A.

Figure 21. - Minimum-stable inlet performance at angle-of-attack.



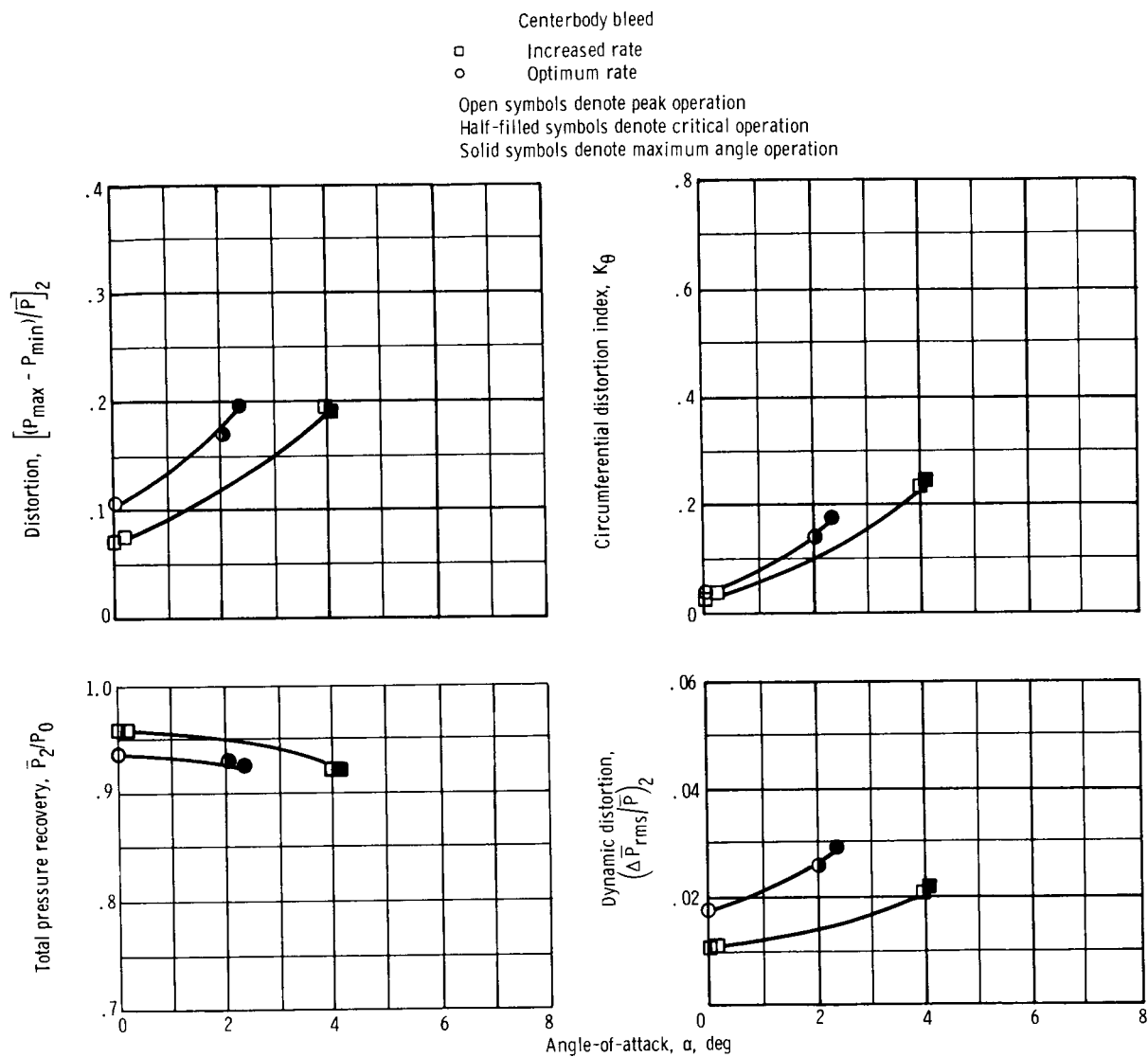
(b) Inlet Mach number, 2.5; configuration Accb.

Figure 21. - Continued.



(c) Inlet Mach number, 2.5; configuration IAcbb.

Figure 21. - Continued.



(d) Inlet Mach number, 2.0; configuration IAcb.

Figure 21. - Concluded.

Ratio of local total pressure to compressor-face average total pressure

:::: 1.150 to 1.100 :::: 1.050 to 1.000 :::: 0.950 to 0.900
 :::: 1.100 to 1.050 :::: 1.000 to 0.950 :::: 0.900 and below

○ Beginning of unstart, minimum stable point without buzz
 □ Unstarted
 △ Just before restart
 ▽ Just after restart
 ◇ Started
 ○ End of unstart sequence, started operation

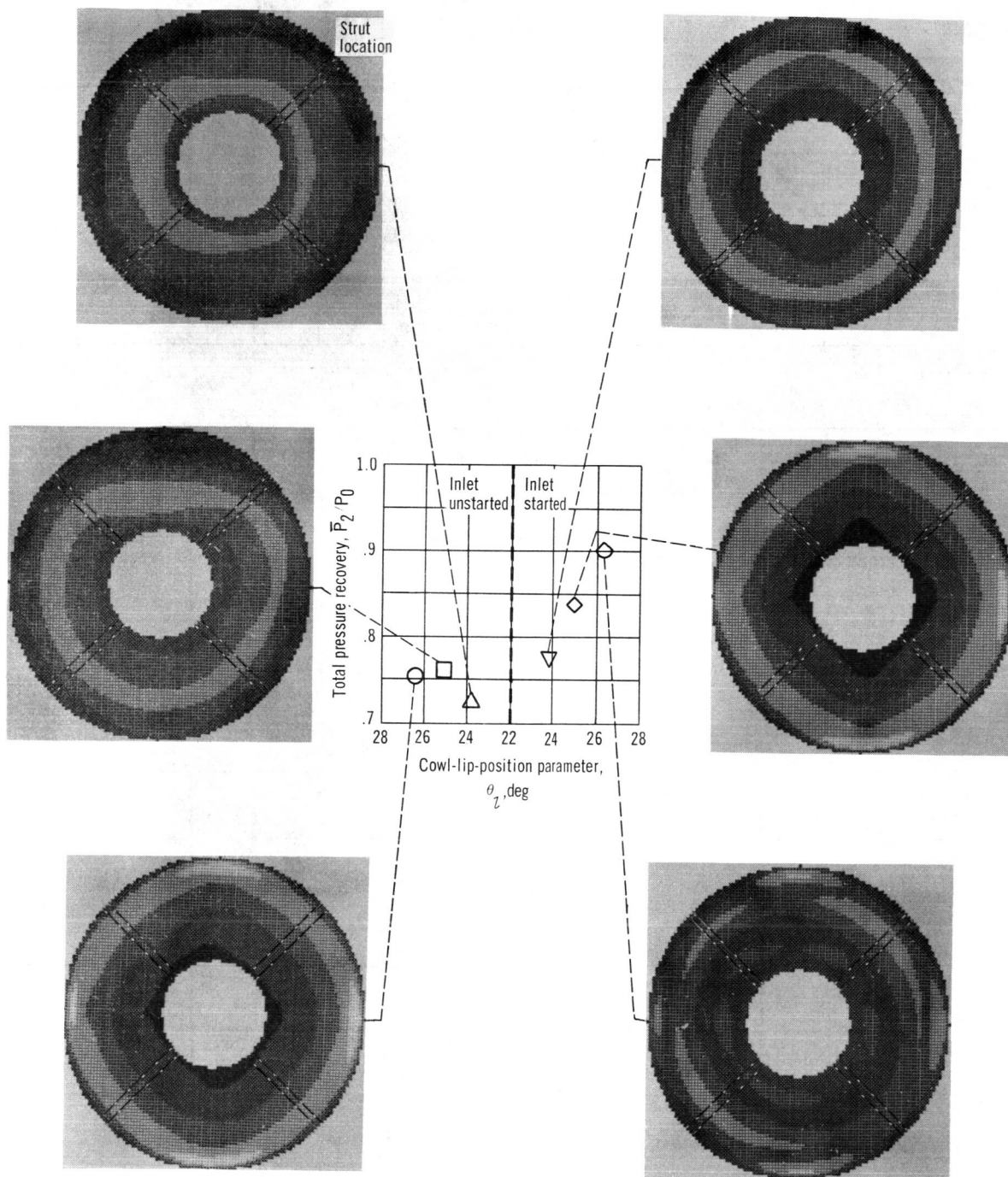


Figure 22. - Variation of steady-state distortion contours and total pressure recovery during unstart-restart sequence. Configuration IAcb; angle-of-attack, 0° ; inlet Mach number, 2.5.

- Beginning of unstart, minimum stable point without buzz
- Unstarted
- △ Just before restart
- ▽ Just after restart
- ◇ Started
- ◇ End of unstart sequence, started operation
- Constant bypass flow area

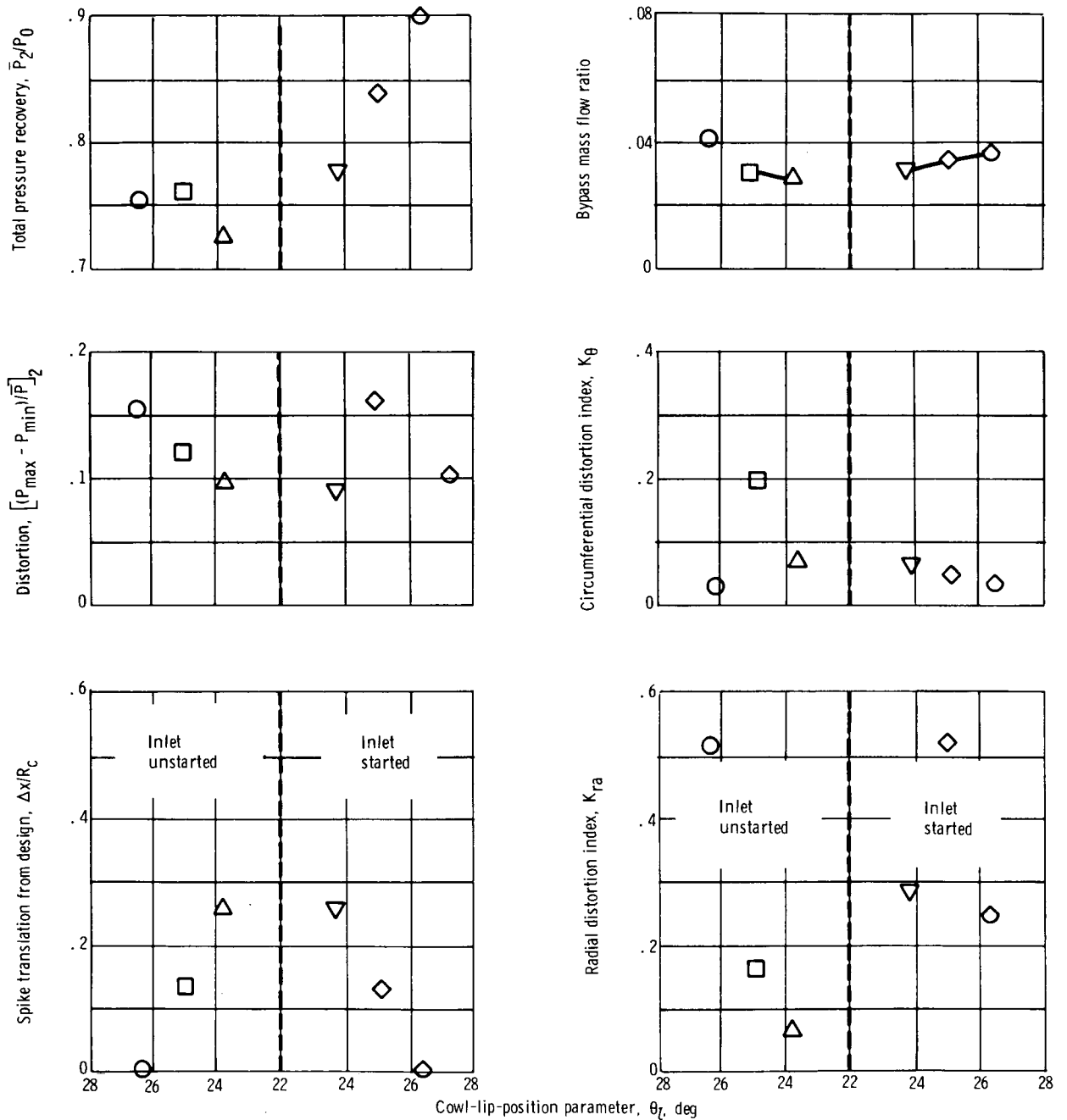


Figure 23. - Variation of steady-state performance with cowl-lip-position parameter. Configuration IAcbb; angle-of-attack, 0° ; inlet Mach number, 2.5.